Available online at www.sciencedirect.com
SCIENCE DIRECT®
International Journal of Rock Mechanics & Mining Sciences 42 (2005) 481–507
International Journal of Rock Mechanics and Mining Sciences
www.elsevier.com/locate/ijrmms

Considerations of the dilatancy angle in rocks and rock masses

L.R. Alejano*, E. Alonso

Natural Resources & Environmental Engineering Department, University of Vigo, Campus Lagoas, ETSI Minas E-36.310, Vigo (Pontevedra), Spain

Accepted 7 January 2005
Available online 14 March 2005

Abstract

The present study responds to the poor treatment given to dilatancy in classical rock mechanics post-failure problems such as tunnel or mine pillar design. A comprehensive review of the literature and observations in regard to published test results would indicate that dilatancy is highly dependent both on the plasticity already experienced by the material and confining stress; moreover, it also appears that scale may play a non-negligible role. In our article, we provide a detailed analysis of published test data with a view to proposing a sufficiently significant but conveniently simple formulation of the dilatancy angle that reflects these dependencies and that can be readily implemented in numerical codes. The model is then tested, demonstrating that it is capable of representing rock sample strain behaviour in compressive tests. Finally, the model is applied to the resolution of ground reaction curves for tunnels in poor-to-average-quality rock masses, showing a good correlation with results obtained using practical rock engineering techniques.

1. Introduction

The importance of a thorough knowledge of the complete stress–strain curve in rock and rock masses has frequently been underlined in the rock mechanics, and most particularly, in earlier breakthroughs [1–3] in the discipline. In the last 30 years, significant success has been obtained in terms of methodologies for estimating reasonably good elastic parameters and failure criteria in rocks, joints and rock masses. However, the difficulties associated with defining a model that adequately reflects observed complete stress–strain curves have affected the possibilities of developing suitably valid approaches for handling post-failure strength behaviour and dilatancy. This problem consistently attracted the attention of early researchers in rock mechanics [2,4,5], and continues to do so in more recent years [6–8]. In routine engineering applications, however, dilatancy seems to receive a great deal less attention, which is hardly surprising since, first of all, many problems in rock mechanics are solved by avoiding failure, and secondly, because of the inherent difficulties in estimating dilatancy.

The aim of the present study is to develop a consistent model for estimating rock mass dilatancy, with potential applications in tunnel and mine design. In view of present trends in modelling [9], the purpose of the study is not to obtain highly accurate values, provide a mirror image of reality, or consider all elements in accurate proportions, but rather to focus on the issues that affect the question of dilatancy in practical engineering problems. The idea follows on from authors like Kudoh et al. [10], who—after modelling a large underground cavern—indicated the need for the plastic properties of the rock mass to be evaluated by including an estimation of dilatancy. Previous studies by the same authors [11] also indicated that limited knowledge of dilatancy was an impediment to understanding particular mechanisms and to achieving modelling objectives.

With the increase in the use of numerical modelling in rock engineering in recent decades, excavation design has come to rely, at least partially, on numerical studies.

*Corresponding author. Tel.: +34 986 81 23 74; fax: +34 986 81 22 01.
E-mail address: alejano@uvigo.es (L.R. Alejano).

1365-1609/$ - see front matter © 2005 Elsevier Ltd. All rights reserved.
doi:10.1016/j.ijrmms.2005.01.003

A review of a number of publications on this topic reveals that dilatancy angle (ψ) is seldom taken into consideration; and when it is considered, the approach is poorly developed and simplistic, generally consisting of an associated flow rule ($\phi = \psi$) or a non-associated flow rule with $\psi = 0^\circ$. Nevertheless, some researchers have remarked that an associated flow rule does not necessarily represent post-failure rock behaviour [7]. Moreover, Detournay [12]—alerting the rock mechanics community as to possible calculation errors when constant dilatancy is assumed—proposed a shear plastic strain-dependent formulation. Although Detournay points out that his proposed flow rule is speculative, the shear plastic strain dependence of dilatancy is, nonetheless, an observable fact. The confining stress-dependent nature of dilatancy has also been pointed to by the same author, among others [12–14], and can also be inferred from a detailed analysis of triaxial tests on rock samples performed in servo-controlled presses [14–16]. What is not so obvious is the scale dependence of dilatancy, which is a hypothesis that remains to be tested [13,17], although largely accepted for rock joint dilatancy [18,19].

In their efforts to improve on existing techniques for obtaining significant rock mass parameters, Hoek and Brown [20]—who have had vast experience in the numerical analysis of a variety of practical problems—recommend the use of dilatancy angle values related to the friction angle and rock mass quality, in the range $\psi = \phi/4$ for good-quality rock to $\psi = 0$ for poor-quality rock. The interesting fact about this approach is that it reflects the significant error induced in a design calculation when a simple associated flow rule is considered. In regard to post-failure behaviour of the material, Hoek and Brown also suggest a transition from brittle to perfectly plastic rock masses for decreasing rock mass quality [21].

Correctly estimating dilatancy is of paramount interest in order to resolve certain post-failure rock mechanics issues, such as the practical problem of modelling underground excavations, as also more theoretical issues, such as shear-band orientation [22]. This explains the interest in developing a methodology that is simple enough for engineering applications and yet provides realistic dilatancy angle values.

2. Definitions

2.1. Constitutive models for rocks and rock masses

A constitutive model of a rock or a rock mass incorporates a series of stress–strain relationships that mark the stress–strain behaviour of the material. Irrespective of the simple elastic part and based on the incremental theory of plasticity [23–25], a material is characterized by a failure criterion $f = 0$ and a plastic potential g. In the broadest sense—in other words, if the model includes hardening or softening—the failure criterion and plastic potential depend not only on the stress tensor σ_{ij}, but also on what is denominated a plastic or softening parameter η, in other words, on the plasticity already experienced by the material.

The failure criterion can be defined as follows:

$$f(\sigma_{ij}, \eta) = 0. \tag{1}$$

Since perfectly plastic behaviour is characterized by a failure criterion that does not depend on the plastic parameter, there is no need to take η into consideration. Strain-softening behaviour is characterized by a gradual transition from a peak failure criterion to a residual failure criterion (located below the peak failure), a transition that is governed by the softening parameter η and which can be implemented in a variety of ways [21,26].

There is a fundamental difference between perfectly plastic models and strain-softening models. Perfectly plastic models can, theoretically, be considered constitutive models, given that they fulfil Drucker's stability postulate [27], which states that the work of the external agency on the displacement produced must be positive or zero. The strain-softening models, on the other hand, do not fulfil this stability postulate, and so observations will be the result of substantial modifications from testing or stressing the material [28]. On this basis, some authors [29–31] do not consider strain softening as specific to the material, but rather the consequence of the behaviour of a structure formed principally by most of the material (rock) being subjected to limited strain and also by narrow bands of another material (broken rock) where large plastic strains occur. Vardoulakis and Sulem [31], for instance, indicate that strong softening behaviour and strong dilatancy are not intrinsic to the material, but are due to the post-bifurcation behaviour of the mechanical system. This does not necessarily contradict the strain-softening continuum approach, since both acknowledge a loss in strength. The question is which type of behaviour model is more suitable. Certain non-associative flow rules can force localization to occur, with the result that a reduction in strength capacity is observed. We propose to incorporate strain softening in our model, thereby demonstrating that it can reproduce the deformational phenomena observed in rock sample testing.

Duncan Fama et al. [32] presented a strain-softening model for analysing coalmine pillar stability that was based on FEM techniques and a modified Hoek and Brown failure criterion, where softening was introduced in accordance with the plasticity level controlled by a softening parameter $\gamma^p = \varepsilon_1^p - \varepsilon_3^p$.

The plastic strain increments can be obtained from the plastic potential:

$$g(\sigma_{ij}, \eta) \tag{2}$$

in accordance with

$$\dot{\varepsilon}_{ij}^{\mathrm{p}} = \dot{\lambda} \frac{\partial g}{\partial \sigma_{ij}}, \tag{3}$$

where $\dot{\lambda}$ is a plastic multiplier and unknown. Eq. (3) is the constitutive equation for the plastic regime and is usually denominated by the flow rule. Incremental plasticity involves the consideration of a fictitious 'time' variable, even if it does not have physical meaning. This variable controls the evolution of plasticity. This 'time' variable called τ, controls the plastic strain increments in the following manner:

$$\dot{\varepsilon}_{ij}^{p} = \frac{\partial \varepsilon_{ij}^{\mathrm{p}}}{\partial \tau}. \tag{4}$$

The final constitutive equation of the plastic regime according to Hill [23] is

$$\dot{\sigma}_{ij} = \left[C_{ijkl}^{\mathrm{e}} - \frac{\langle 1 \rangle}{H} \left(\frac{\partial g}{\partial \sigma_{mn}} C_{mnij}^{\mathrm{e}} \frac{\partial f}{\partial \sigma_{\mathrm{rs}}} C_{\mathrm{rs}kl}^{\mathrm{e}} \right) \right] \dot{\varepsilon}_{kl}, \tag{5}$$

where $\langle 1 \rangle$ stands for 0 or 1, depending on whether the increment is purely elastic ($\dot{\lambda} = 0$) or also contains plastic terms ($\dot{\lambda} > 0$). H is the plastic modulus and it can be subdivided into two, in such a way that $H = H_0 + H_t$; where H_0 coincides with the plastic modulus of the perfectly plastic behaviour and H_t is known as the hardening/softening modulus

$$H_0 = C_{ijkl}^{\mathrm{e}} \frac{\partial f}{\partial \sigma_{ij}} \frac{\partial g}{\partial \sigma_{kl}}, \quad H_t = -\frac{\partial f}{\partial \eta}. \tag{6}$$

The classification of the post-failure behaviour is made according to the value taken by these plastic moduli in such a way that if $H_t > 0$ the material is a strain-hardening one, if $H_t < 0$ the material is a strain-softening one, if $H_t = 0$ the material is perfectly plastic and finally if $H = H_0 + H_t = 0$ the material is purely brittle.

Obviously, these moduli depend on the failure criterion and on the flow rule selected, and according to the cases, a material can behave differently for different levels of confinement.

If the plastic potential coincides with the failure or yield criterion ($f \equiv g$), then the material is said to obey the normality rule, since the plastic strain increment vector is normal and moves outwards from the failure surface. Alternatively, a material can be said to obey an associated flow rule when the nature of the deformation is linked to the failure surface. Normality and associated flow are equivalent terms; naturally, when working with material behaviour models, it is clearly useful if we can assume the failure criterion and plastic potential forms to be the same, since the number of functions needed to model the plastic response will be reduced by one. Some authors [7] disregard associated flow rules since, theoretically, these involve plastic deformation without energy dissipation, which is inconceivable.

Although normality (or minor deviations from normality) can be reasonably assumed for clayey soils [33,34], it is clear that for many materials—such as granular soils, rocks and rock masses—the plastic potential and failure criteria that are usually proposed cannot be considered identical [7,33]. Non-associated plasticity entails the introduction of a dilatancy angle ψ, which controls inelastic volume changes. This angle would appear to be useful not only for soils, but also for rocks [7].

One of the simplest and most commonly used plastic potential assumptions states that

$$g(\sigma_{ij}, \eta) = \sigma_1 - K_\psi(\sigma_{ij}, \eta) \cdot \sigma_3, \tag{7}$$

where

$$K_\psi(\sigma_{ij}, \eta) = \frac{1 + \sin \psi(\sigma_{ij}, \eta)}{1 - \sin \psi(\sigma_{ij}, \eta)} \tag{8}$$

and where ψ is the dilatancy angle.

In strain-softening behaviour models, a softening parameter η controls strength capacity [32]. However, if we hold Detournay's [12] statements on dilatancy to be valid, then this parameter also controls the flow rule. Although η can be defined in a number of ways, so far there has not been wide support among researchers for any single one of its possible forms, and on many occasions, they are computed in parallel.

Two of the more common definitions of this parameter are that it is a function of internal variables and that it is incremental [7,26]. In the former, for planar deformations in which $\varepsilon_2 = \varepsilon_2^{\mathrm{p}} = 0$, the plastic parameter is based on internal variables. The most widely used variable is shear plastic strain, obtained as the difference between the major and minor principal plastic strains, as follows:

$$\gamma^{\mathrm{p}} = \varepsilon_1^{\mathrm{p}} - \varepsilon_3^{\mathrm{p}}. \tag{9}$$

It is appropriate to indicate that we use the sign conventions of traditional rock mechanics (compression and contraction are taken as positive stress and strain values). To avoid sign convention problems, some authors [7] have applied the above formula in absolute value terms, as follows:

$$\gamma^{\mathrm{p}} = |\varepsilon_1^{\mathrm{p}} - \varepsilon_3^{\mathrm{p}}|. \tag{10}$$

For incrementally defined plastic parameters, the literature provides examples of incremental softening parameters $\dot{\eta}$ [7] that depend on plastic strain

increments, with the most widely used defined as

$$\dot{\eta} = \frac{\Delta\eta}{\Delta\tau} = \sqrt{\frac{2}{3}\left[\dot{\varepsilon}_1^p\dot{\varepsilon}_1^p + \dot{\varepsilon}_2^p\dot{\varepsilon}_2^p + \dot{\varepsilon}_3^p\dot{\varepsilon}_3^p\right]} \tag{11}$$

The FLAC code [26], based on FDM, implements an incremental plastic parameter e^{ps} and focuses on plane strain conditions, whose incremental form is

$$\Delta e^{ps} = \left\{\frac{1}{2}(\Delta\varepsilon_1^{ps} - \Delta\varepsilon_m^{ps}) + \frac{1}{2}(\Delta\varepsilon_m^{ps})^2 + \frac{1}{2}(\Delta\varepsilon_3^{ps} - \Delta\varepsilon_m^{ps})2\right\}^{1/2}, \tag{12}$$

where $\Delta\varepsilon_m^{ps} = \frac{1}{3}(\Delta\varepsilon_1^{ps} + \Delta\varepsilon_3^{ps})$ and $\Delta\varepsilon_j^{ps}$ $j = 1, 2, 3$ are the principal shear plastic strain increments. This incremental plastic parameter can be correlated with the more standard γ^p or plastic shear strain. If an elastoplastic strain-softening material with a constant dilatancy angle is considered—characterized by a plastic potential as in Eqs. (8), (9) and (12)—then the following relationship between $\gamma^p$and e^{ps} can be deduced [35]:

$$e^{ps} = \frac{\sqrt{3}}{3}\sqrt{1 + K_\psi + K_\psi^2}\,\frac{\gamma^p}{1 + K_\psi}. \tag{13}$$

For null dilation, as proposed by some authors [20] for particular rock masses, Eq. (13) becomes

$$e^{ps} = \gamma^p/2. \tag{14}$$

When dilatancy is not considered to be constant, this relationship should be calculated only as the deformation process unfolds. Nonetheless, from our analyses we can conclude that the use of Eq. (14) produces negligible errors.

2.2. Dilatancy

Dilatancy can be defined as a change in volume resulting from the shear distortion of an element in a material. As Eqs. (7) and (8) demonstrate, the dilatancy angle ψ is a suitable parameter for describing the behaviour of a dilatant material, since it represents the ratio of plastic volume change to plastic shear strain. Strictly speaking, this definition of ψ is only valid in the case of pure shear [7], as the flow rule is then totally controlled by ψ, which at the same time defines the volume increase or dilation of the rock or rock mass following failure.

For granular soils, rocks and concrete, Vermeer and de Borst [7] point to a dilatancy angle that is significantly smaller than the friction angle. These authors proposed the following equation for assessing the dilatancy angle in its more general form:

$$\psi = \arcsin\frac{\dot{\varepsilon}_v^p}{-2\cdot\dot{\varepsilon}_1^p + \dot{\varepsilon}_v^p}. \tag{15}$$

The advantage of this formulation, as the authors have indicated, resides not only in the fact that it commences with the plastic volumetric strain rate and is also valid for the interpretation of triaxial tests, but that it can be applied to the analysis of plane strain conditions, and even in true triaxial situations. It should be pointed out that the fraction denominator represents, in absolute terms, the plastic parameter defined from internal variables (as in Eq. (9)).

For a standard triaxial test in which confining stress is applied to a sample peripherally, it is clear that, under homogeneous deformation conditions, $\varepsilon_2 = \varepsilon_3$, and so $\varepsilon_v = \varepsilon_1 + 2\cdot\varepsilon_3$. In this case the value of the relationship $-\mathrm{d}\varepsilon_3^p/\mathrm{d}\varepsilon_1^p$ equal to $1+\sin\psi/1-\sin\psi$, is now equal to $2K_\psi$. Thus, dilatancy in triaxial tests can be also computed from

$$\sin\psi = \frac{\dot{\varepsilon}_1^p + 2\dot{\varepsilon}_3^p}{-\dot{\varepsilon}_1^p + 2\dot{\varepsilon}_3^p} \tag{16}$$

from which we obtain (for triaxial tests only):

$$\dot{\varepsilon}_3^p = \frac{1}{2}\frac{1+\sin\psi}{1-\sin\psi}(-\dot{\varepsilon}_1^p) = \frac{K_\psi}{2}(-\dot{\varepsilon}_1^p). \tag{17}$$

Hence, the formula $-(\dot{\varepsilon}_3^p/\dot{\varepsilon}_1^p)$, which gives the slope of the curve that relates plastic radial and axial strains in the plastic deformation stage in the complete stress–strain curve (Fig. 1), can be interpreted in accordance with

$$-\frac{\mathrm{d}\varepsilon_3^p}{\mathrm{d}\varepsilon_1^p} = \frac{1}{2}\frac{1+\sin\psi}{1-\sin\psi} = \frac{K_\psi}{2}. \tag{18}$$

From triaxial test results for rock samples, it is thus possible to analyse dilatancy starting from the values σ_1, σ_3, ε_1 and ε_3, and provided that Young's modulus E and Poisson's ratio v are known. Decomposition of total strains into their elastic and plastic parts $\varepsilon_i = \varepsilon_i^e + \varepsilon_i^p$ should be taken into account, as also the possibility of obtaining the elastic parts for these strains starting from the elastic constants.

Nevertheless, the analysis of dilatancy angles from a standard triaxial compression test perspective encounters difficulties associated with: the inelastic behaviour of the stress–strain curve; variability in the elastic parameters; and the occurrence of non-homogeneous deformation modes (bifurcation and subsequent axial splitting and shear banding). This would indicate that the results of such tests should be used with caution. This problem has led to the definition of new tests specifically designed to estimate dilatancy [36].

For the case of plane strain, for instance, in order to interpret measurements for a section of tunnel, if the measured strains are ε_v and ε_1, and given $\varepsilon_2 = 0$, then $\varepsilon_v = \varepsilon_1 + \varepsilon_3$. So the value of the relationship $-\mathrm{d}\varepsilon_3^p/\mathrm{d}\varepsilon_1^p$ will be equal to $1+\sin\psi/1-\sin\psi$ and therefore to K_ψ, which is the slope of the relationship between the plastic

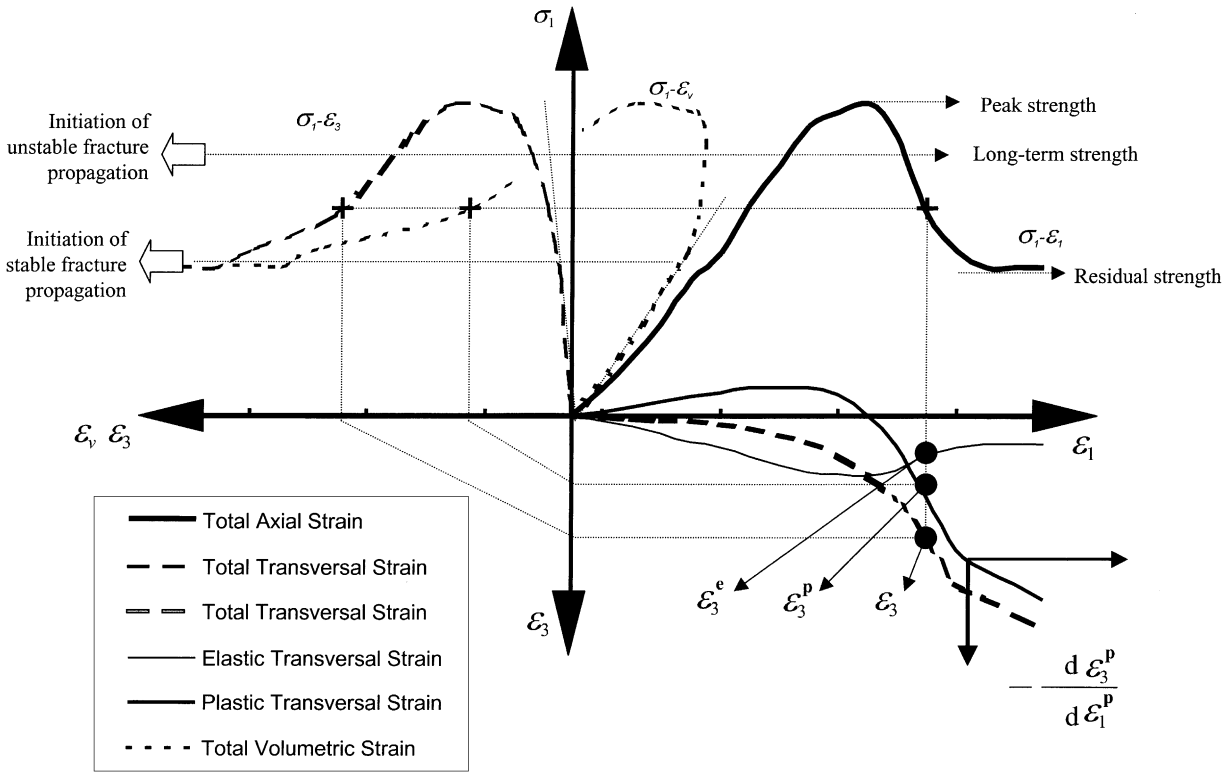

Fig. 1. Complete stress–strain curve for a test on rock. It includes the axial stress vs. axial, radial and volumetric strain on the one hand and the total, elastic and plastic radial strain vs. the axial strain on the other.

hoop and radial strains (See [7] for further details of this formula).

It is important at this juncture to be aware of some of the issues raised as a result of investigating complete stress–strain curves in rock masses [1,3]. Between the initiation of stable fracture propagation and the onset of unstable fracture propagation, ε_3^p is a negative value, whereas ε_1^p is null—in other words, there is no inelastic axial strain (Fig. 1). For initial small values for the plastic parameter, what this means is that the dilatancy angle tends to minus infinity. Other inelastic and non-strictly plastic effects—such as crack closure in the early stages of stress application (resulting in the initial concave form of the stress–strain curve), and rock damage over long-term peak stress (see Fig. 2)—add to the difficulty of obtaining 'accurate' dilatancy values. Given that our aim is to identify general behavioural trends rather than highly accurate values, these effects will be ignored in our analysis. The concept of dilatancy as defined above only makes sense in the post-failure zone, even if at the peak strength point, the plastic parameter is in the order of some mstrains and the inelastic volumetric strain attains values in the range 0.04% to over 0.1% (according to the tests in certain rocks [37]).

3. Preliminary observations

To provide some background to the dilatancy approach developed in this paper, we review here observations and proposals made by a range of authors in regard to dilatant behaviour and dilatancy angles in rocks, rock joints and rock masses.

3.1. Rocks

The earliest proposals concerning dilatancy focused on an associated flow rule (probably due, at least in part, to the simplicity of this hypothesis), which can be observed, for instance, in descriptions of material behaviour models for the axisymmetric tunnel problem [38].

Vermeer and de Borst [7] analysed various rock sample tests and tested different constitutive rock models in order to show that plastic yielding accompanied by a plastic volume increase can describe rock behaviour reasonably well. They concluded that the dilatancy angle is at least 20° less than the friction angle, a conclusion that lends to the use of a non-associative flow rule. This explains the common practice of applying

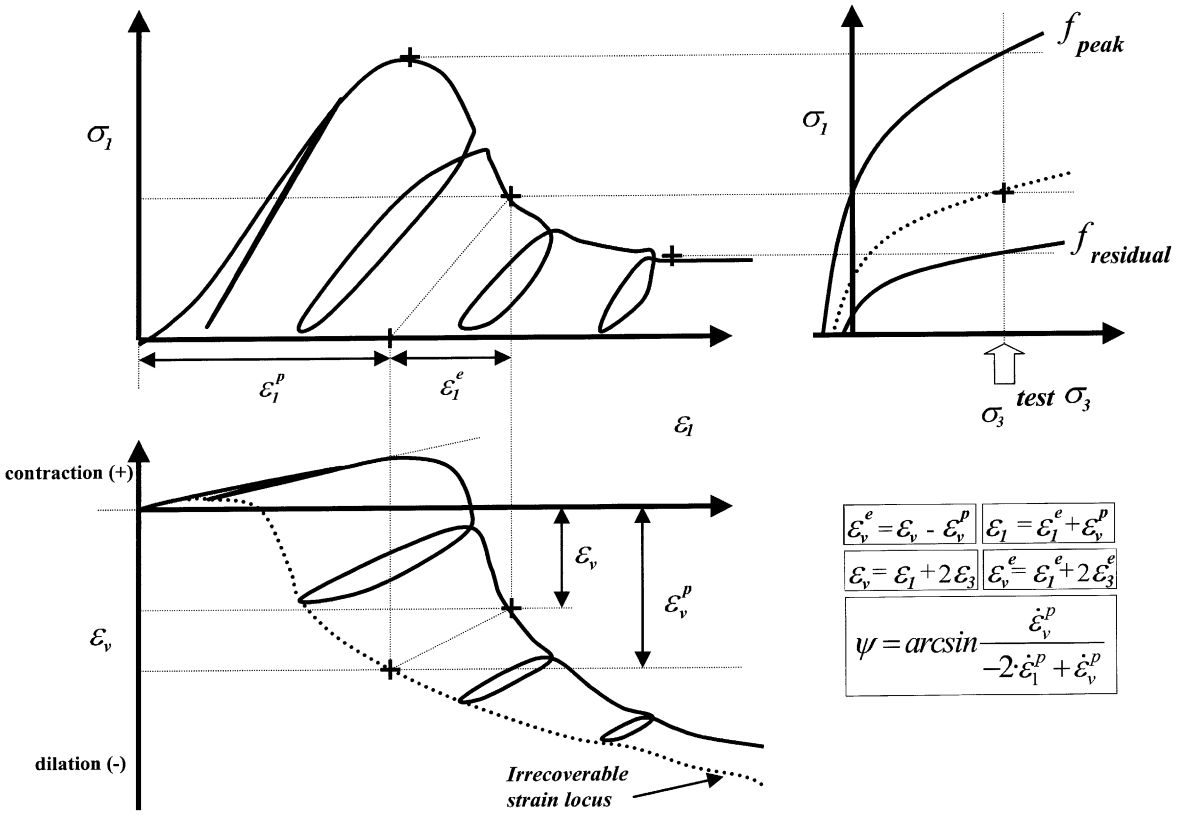

Fig. 2. Stress–strain relationships (axial stress–axial strain in the upper part and volumetric strain–axial strain in the lower part) for a compressive test on a strain-softening coal sample with three unloading–loading cycles. The last graph represents the curve relating the plastic components of the volumetric and axial strain or irrecoverable strain loci, together with the formulation on which it is based. The peak and residual failure criteria are also included (upper right-hand side). *Source*: Adapted from Ref. [16].

a rule-of-thumb dilatancy angle value in the range $\psi = \phi - 20^\circ$ [39].

Detournay [12] was the first to point to the unrealistic and misleading nature of a constant dilatancy angle assumption. He argued that dilatation must of necessity be a function of plastic strain and confining stress, and subsequently proposed a dilatancy factor K_ψ that decays from an initial value K_ϕ in accordance with an exponential function of plastic shear strain, as follows:

$$K_\psi = 1 + (K_\phi - 1)\cdot e^{-\gamma^p/\gamma^{p,*}}, \tag{19}$$

where the parameter $\gamma^{p,*}$ can most usefully be related to the maximum inelastic volume increase Δ^* as

$$\gamma^{p,*} = \Delta^* \Big/ \ln\frac{(K_\phi - 1)}{2}. \tag{20}$$

The author comments on the fact that the number of parameters necessary for the model is the same as for the constant dilatancy case. This interesting and relatively simple flow rule does not appear to be much used in practice.

In his doctoral thesis, Medhurst [40] performed a large number of triaxial tests on multi-scale coal samples (61, 101, 146 and 300 mm in diameter). He pointed to the steady decrease in dilation as confining pressure was increased, and attributed this decrease to the transition from an axial splitting mode to a shearing failure mode in the samples. Other authors [22,41] observed similar effects, but arrived at the opposite conclusion, i.e. they attributed failure mode and shear-band inclination to decreasing dilatancy with confining stress.

Medhurst [40], moreover, did not observe scale dependence in the deformation behaviour of the three largest sample sizes in his study. Concluding that coal samples behave in a non-associated manner, he observed a tendency towards a greater departure from the normality condition as confining pressure increased. The inclusion of loading–unloading cycles in Medhurst's triaxial tests represented an experimental evaluation of the division of volumetric strain into its elastic (or recoverable) and plastic (or irrecoverable) parts (Fig. 2). Results were plotted in terms of $d\varepsilon_1^p/d\varepsilon_3^p$ vs. σ_3 so as to provide sufficient evidence for developing a stress-dependent non-associated flow rule. He used a function of the plastic potential taking the same form as the modified Hoek and Brown failure criterion.

Ribacchi [39], who carried out a large number of standard triaxial tests on limestone samples

characterized by variable fractures, treated the rock sample he tested as a small-scale model of a jointed rock mass. The overall dilatancy angle averages obtained revealed a regular decrease in the dilatancy angle as confining stress was increased. Peak dilatancy angles of roughly 24°, 19°, 16° and 11° were estimated for confining pressures of 2.5, 5, 10 and 20 MPa, respectively.

Medhurst's results [40], as also those of Farmer [15], among others [39], are reinterpreted in the following sections in order to obtain dilatancy angle values and assess dilatancy dependencies on different parameters.

3.2. Joints

It has been observed that failure in rock or rock masses takes place in joints, shear zones or bands. The macroscopic behaviour of the rock or rock mass must, thus, be related in some way to shear zone or joint behaviour.

Barton and his colleagues [18,19] studied natural rock joints in detail. From a classic graph showing the dilatant behaviour of a joint in a shear test (Fig. 3) [41], it was peak dilatancy that appeared to be associated with joint peak shear strength, and could, moreover, be defined for joints as the peak slope of the relationship $\delta v/\delta h$, where δh and δv are, respectively, shear and normal displacements measured for the discontinuity. Beyond peak strength, this relationship flattens out. Hence, joint dilatancy can be calculated for each point in the graph as

$$d_n = \arctan\left(\frac{\delta_v}{\delta_h}\right). \tag{21}$$

According to Barton and Bandis [19], peak joint dilatancy angle can be estimated using the expression:

$$d_{n,\text{peak}} = JRC \log_{10} \frac{JCS}{\sigma_n}, \tag{22}$$

where the actual values of the joint roughness coefficient (JRC) and the joint compressive strength (JCS) should be scale-corrected, according to the expressions:

$$JRC_n = JRC_0 \left(\frac{L_n}{L_0}\right)^{-0.02\,JRC_0} \quad \text{and}$$

$$JCS_n = JCS_0 \left(\frac{L_n}{L_0}\right)^{-0.03\,JRC_0}, \tag{23}$$

where L_n is the actual joint length and L_0 is the reference joint length (equal to 1 m).

From this formulation it can be deduced that, for the case of a joint (and, as we shall see below, extrapolation to the study of rock masses is also possible), peak joint dilatancy decreases when normal stress σ_n (σ_3 for rocks)

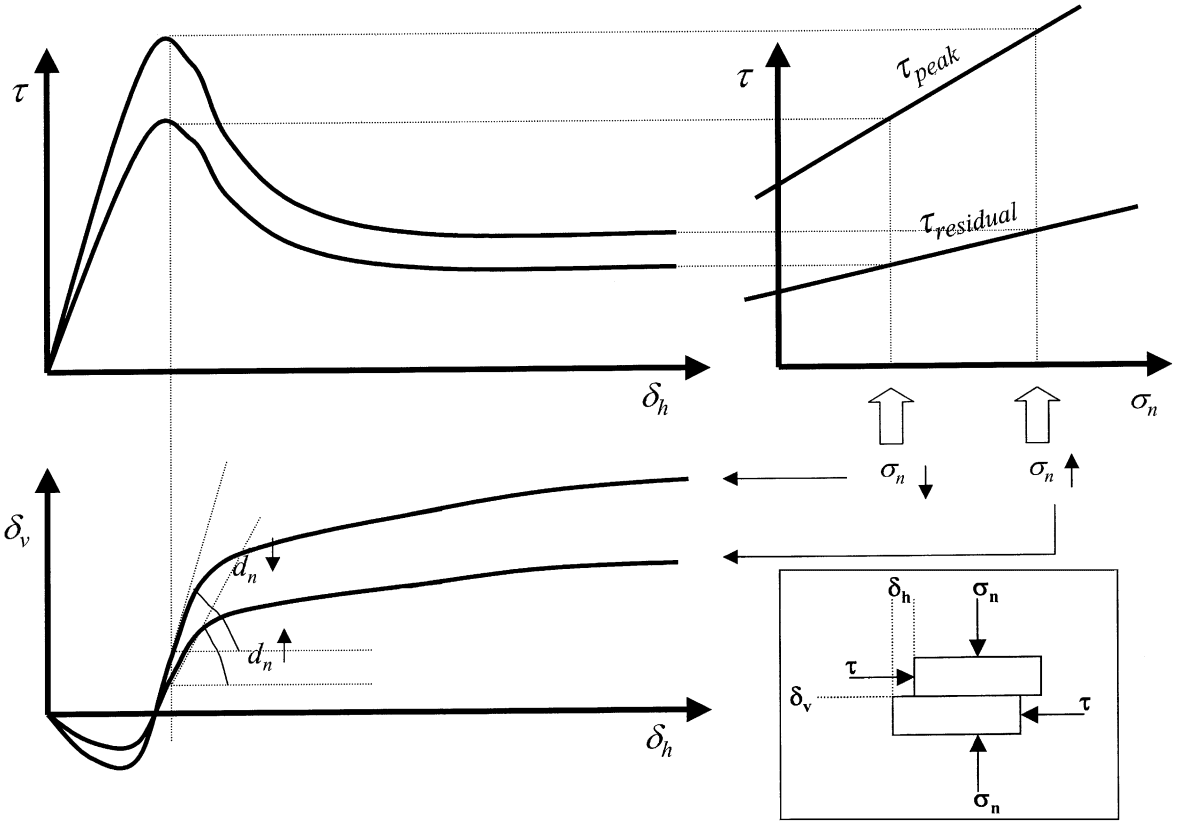

Fig. 3. Stress–strain curves of a rock joint for increasing normal stress and including the relationship between normal and shear displacement. *Source*: Adapted from Ref. [42].

is increased, with increasing joint scale (sample diameter for rocks), decreasing *JCS* (σ_c for rocks) and decreasing *JRC* (grain size, failure mode and friction angle). For larger scales, the impact on *JCS* and *JCR* is usually negligible. These relationships are all coherent from a mechanistic perspective. Finally, even if the Barton–Bandis model [19] deals only with peak dilatancy, it seems reasonable to suppose that joint dilatancy tends to a null value, given that the volume of a sample cannot increase to infinity.

Although it may seem odd that we propose extrapolating—as suggested above—from joints to rock masses, we are, in fact, following Archambault et al. [13]. These authors reviewed the different factors contributing to progressive failure in rock and rock masses and demonstrated how shear or tension discontinuity anastomosing structures and scale effects in shear rock strength are the result of a progressive softening of the rock or rock mass. Moreover, the application of shear stresses generates simple shear strains that are non-homogeneous and non-coaxial with the medium. This produces a concentration of shear or tensile stress in thin bands or zones where deformation is localized and where the tensile or shear fracture propagation commences. The development of these fractures corresponds to a hardening stage characterized by increased dilatancy that involves the growth of the shear zone. Following a full propagation of these discontinuities up to an upper shear-stress limit, an unstable softening region is entered and new discontinuities appear. When residual strength is attained, anastomosed discontinuity structures, in which softening is concentrated, start to form. Furthermore, the same authors show how these conclusions are valid for scales ranging from millimetres to thousands of miles. The macroscopic behaviour of the whole rock mass responds to Fig. 4 in terms of stress, strain and dilatancy for different scales.

3.3. Rock masses

Most of the researchers who have studied dilatancy in rock and rock masses have acknowledged the need to use non-associative flow rules [7,12,15,17,20,43].

Given that the performance of significant tests on rock masses is a complex matter, dilatancy studies should be based on field experiments and back-analysis, even though it has to be acknowledged that neither is particularly convenient. Based on wide practical rock engineering experience and probably inspired by the idea of providing the rock mechanics community with parameters for feeding numerical models, Hoek and Brown [20] recommended the use of constant dilatancy angle values based on rock mass quality; they proposed,

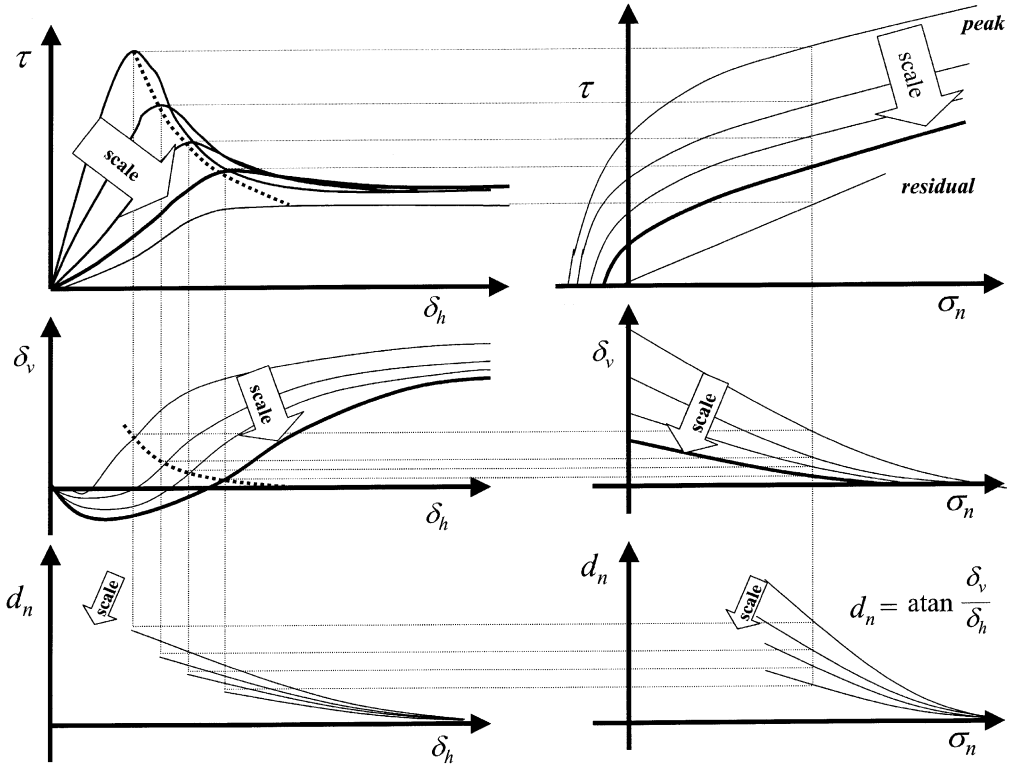

Fig. 4. Shear stress–strain behaviour of rock masses with increasing scale, based on Archambault et al. [13]. Note that these authors indicate that this behaviour can be observed for all scales, ranging from millimetres to hundreds of kilometres. The top four graphs are based on Ref. [13] and the two lower graphs were extrapolated from these.

thus, values of $\psi = \phi/4$ for excellent- and good-quality rock masses, $\psi = \phi/8$ for average-quality rock masses and $\psi = 0$ for poor-quality rock masses. This is not, in fact, a general proposal, but a calculated guess applied to particular rock mass cases on the basis of expert opinion on dilatant behaviour in rock masses.

Referring to the post-failure behaviour of rock masses, Hoek and Brown's [20] general guidelines recommend attributing brittle post-failure behaviour to excellent- and good-quality rock masses, strain-softening behaviour to average-quality rock masses and perfectly plastic behaviour to poor-quality rock masses. This affects the issue of a coherent representation of dilatancy, as a suitable definition of the evolving and decaying failure criteria that define strain softening requires a reference plastic parameter to which these criteria can be associated [32].

4. Test reinterpretation

The test procedure typically adopted in triaxial testing is not suitable for assessing rock dilation characteristics. This is because volumetric strains are not directly determined but must be estimated on the basis of the transversal strain along one diameter. Moreover, stress–strain curves from triaxial tests have peaks that are partially a consequence of thin shear bands. Strain measurements for such macroscopic non-uniform deformations are not objective, unlike those for the axial strain–volumetric strain curve, which are much more accurate. Although it may not be possible to accurately measure the magnitude of the strain increment, the strain ratio is not so strongly affected by the effects resulting from the location of a shear band [7]. Hence, even though tests have been defined [36] that accomplish this task in a more rigorous way, dilatancy angles may be measured with acceptable accuracy despite the non-uniformity of the deformation.

The approach described here does not directly address the issue of strain localization, given that strain measurements in the information gathered from tests and the associated calculations assume uniform or average behaviour in the samples.

In the next section, a range of tests published in the literature will be reanalysed in the light of the definitions given above—in particular, the set of tests performed on coal samples by Medhurst [40] and some of the tests performed by Farmer [15]. It should be pointed out that the data corresponding to these tests were published in the form of graphs, so the accuracy of the figures recovered from these graphs and used for this reinterpretation may not be very high. However, we consider such inaccuracies to be of little significance, given that the final results will not be used dogmatically to fit exact curves but to identify behavioural trends that can be adapted to more general observations.

4.1. Reinterpretation of Medhurst's tests on coal samples

Medhurst [40] performed an exhaustive and highly reliable series of triaxial compression tests on 61, 101, 146 and 300 mm coal samples using a servo-controlled press. For some samples—including most of the larger ones—loading–unloading cycles were included as part of the testing procedure and recoverability curves were created. Monitoring oil displacement in the triaxial cell during these tests, Medhurst devised an alternative method for recording volumetric strain behaviour in deformed coal, which ultimately proved more accurate than the strain-gauged methods. Although this method was better at obtaining averages, it tended to conceal non-homogeneous deformation modes. The reason why these tests were chosen for this study is that they are unique in providing information on scale effects in the complete stress–strain curve for coal. The irrecoverable strain loci for many of the tests were extrapolated to our case (see Fig. 2) and, applying Eqs. (15) and (9), were used to calculate both the dilatancy and plasticity experienced by the sample (the plastic parameter) at different stages of the deformational process. An additional advantage of these tests is related to the fact that coal presents small-scale jointing or 'cleating', associated with its brightness. Test-scale coal behaves very much like a rock mass structure, and so compressive tests on relatively large (300 mm diameter) samples can be considered to reflect small-scale rock masses.

For each test, Medhurst [40] obtained a total for strain relationships (ε_v vs. ε_1). For most of the tests on larger samples (146 and 300 mm in diameter)—performed with loading–unloading cycles—the ε_v^p vs. ε_1^p curves (or irrecoverable strain loci) were also estimated. To carry out our study, ε_v^p and ε_1^p values were first obtained for particular intervals—typically 1 to 2 mstrain—from the corresponding graphs in Medhurst's thesis. From these values the plastic transversal strain for each point in each test was calculated as

$$\varepsilon_3^p = (\varepsilon_v^p - \varepsilon_1^p)/2. \tag{24}$$

Next, the average values of ε_1^p and ε_3^p for each interval were computed, together with the corresponding increments in the plastic axial and volumetric strains $-\Delta\varepsilon_1^p = \dot{\varepsilon}_1^p$ and $-\Delta\varepsilon_v^p = \dot{\varepsilon}_v^p$. The corresponding plasticity parameters were then calculated from average values using Eq. (9). Finally, Eq. (15) was used to calculate the dilatancy angle. Obtained for each test were pairs of values for the dilatancy angle ψ and the plasticity parameter γ^p that could be represented in graph format.

For very low initial values for the plasticity parameter, the dilatancy angle was negative or highly negative in all the reinterpreted tests, as can be deduced

from the $\varepsilon_v^p - \varepsilon_1^p$ curve in Fig. 2, or from comments on complete stress–strain curve behaviour between the onset of stable and unstable fracture propagations, in the compressive test stage traditionally known as dilatancy onset. Paradoxically, this test phase ($\Delta\varepsilon_1^p = 0$ and $\Delta\varepsilon_3^p < 0$) is disregarded in our model, but we feel this to be necessary in view of our aim for simplicity, and also due to the fact that initial volumetric strain behaviour is usually negligible anyway, when compared to final plastic volumetric strain. From these initial negative values, thus, the dilatancy angle increases rapidly to a peak value and then decreases monotonically. In our graphs, the relationship between the dilatancy angle ψ and the plasticity parameter γ^p is only plotted starting from a relatively high value for dilatancy, i.e. we have ignored the initial zone, which tends to include very few intervals.

Two series of Medhurst tests [40] were analysed and represented. The first series was used to study the role of confining stress on dilatancy; therefore, triaxial compression tests were performed on large samples (146 and 300 mm diameter), which were subjected in turn to confining stresses of 0.2, 0.2, 0.4, 0.8, 1, 3, 4 and 4 MPa. The second series, which was used for investigating scale effects, included triaxial compression tests performed with a confining stress of 0.2 MPa applied to 61, 101, 101, 146, 146 and 300 mm diameter samples. These results are illustrated in Figs. 5 and 6, respectively. Note that the results for the latter should be considered less reliable, given that the irrecoverable strain loci for the smaller specimen tests were estimated from the $\varepsilon_v - \varepsilon_1$ curve.

The reinterpreted results in Figs. 5 and 6 should be used with caution, given possible inaccuracies in the

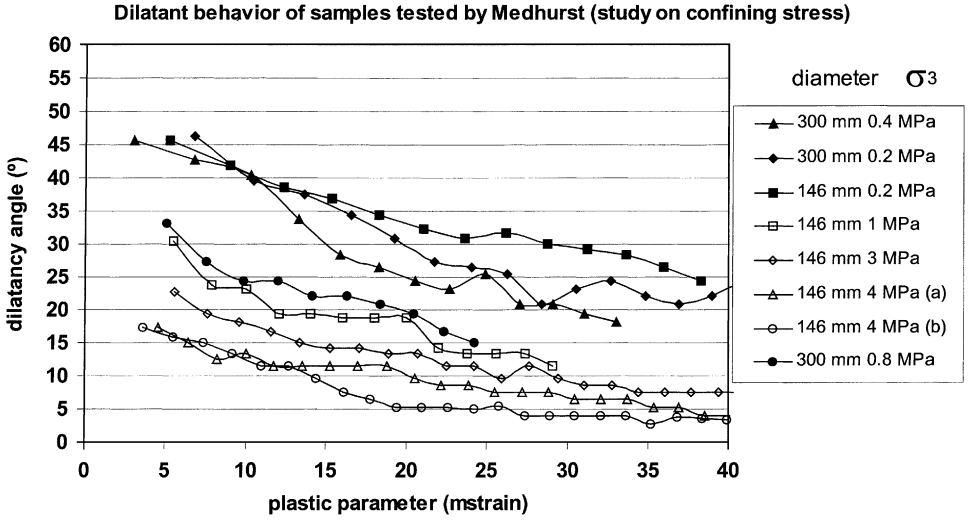

Fig. 5. Dilatancy angle–plastic parameter relationships obtained by reinterpreting a series of triaxial compressive tests by Medhurst [40] on large samples (146 and 300 mm) submitted to confining stresses of 0.2, 0.2, 0.4, 0.8, 1, 3, 4 and 4 MPa.

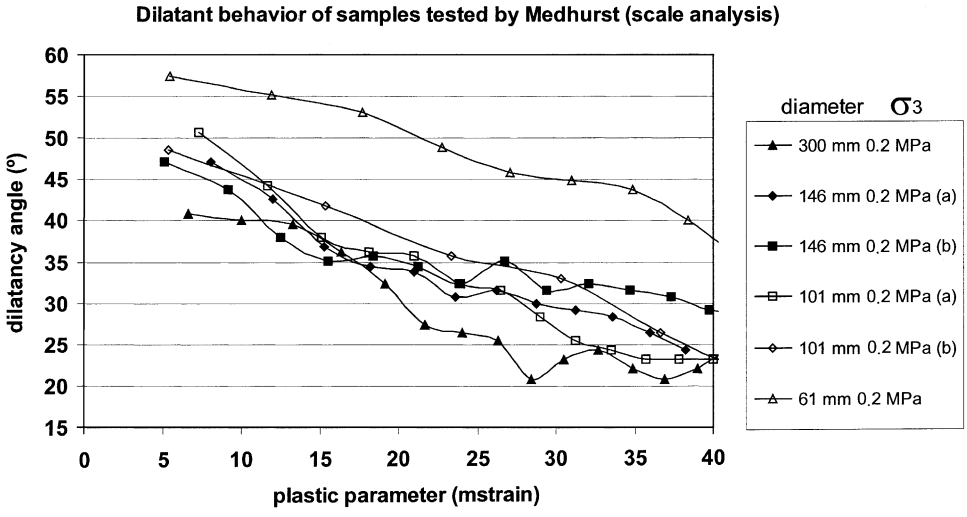

Fig. 6. Dilatancy angle–plastic parameter relationships obtained by reinterpreting a series of triaxial compressive tests by Medhurst [40] on 61, 101, 101, 146, 146 and 300 mm diameter samples submitted to confining stress of 0.2 MPa.

estimation process resulting from having obtained the values from graphs. The dilatancy angles recovered from the graphs give the lowest value for the plastic parameter as a point close to the point of maximum compressive strength; from this point onwards the dilatancy angle tends to decrease exponentially as the plastic parameter increases. This maximum value for the dilatancy angle shall henceforth be denominated 'peak dilatancy' in this article.

In relation to Figs. 5 and 6, some further comments are in order. First of all, dilatancy tends to decrease as the plasticity experienced by the sample increases; moreover, peak dilatancy seems to diminish as confining stress and scale increase. It seems clear, then, that a proper formulation of dilatancy should include plastic parameter, confining stress and scale dependencies, in order to adequately represent observed macro-trends, an observation that is reinforced in the literature (see Section 3).

4.2. Reinterpretation of Farmer's tests on different rock types

With the aim of obtaining further information on dilatancy and in line with the definitions described in Section 2, we reinterpreted the results of Farmer's standard triaxial servo-controlled tests on standard samples of predominantly weak rock [3,15]. These tests included different confining stresses, as well as graphs of total axial strain–total volumetric strain curves. The estimated values for the elastic constants, Young's modulus E, and Poisson's ratio v were given. The series of tests reinterpreted here include only those referring to sandstone, silty sandstone, mudstone and Portland stone. The other tests are excluded because of the time-dependent behaviour of the material (rock salt) and/or the paucity of recoverable data.

In this case, given that the irrecoverable strain locus or $\varepsilon_v^p - \varepsilon_1^p$ curve for each test was missing, it had to be estimated. Thus, the elastic axial and volumetric strains for each point recovered from the graph were first calculated in accordance with elasticity theory:

$$\varepsilon_1^e = \frac{\sigma_1 - 2v\sigma_3}{E} \quad \text{and} \quad \varepsilon_v^e = \frac{(1-2v)\sigma_1 - 2(1-v)\sigma_3}{E}. \tag{25}$$

The corresponding plastic values were next obtained by subtracting the elastic part from the total strain corresponding to each point selected, in accordance with

$$\varepsilon_1^p = \varepsilon_1 - \varepsilon_1^e \quad \text{and} \quad \varepsilon_v^p = \varepsilon_v - \varepsilon_v^e. \tag{26}$$

In this way, we obtained more or less reliable irrecoverable strain loci. Applying the same technique used for Medhurst's tests, the corresponding $\psi - \gamma^p$ curve was obtained for each graphed test of the series. The results are represented in Figs. 7a–d. These results

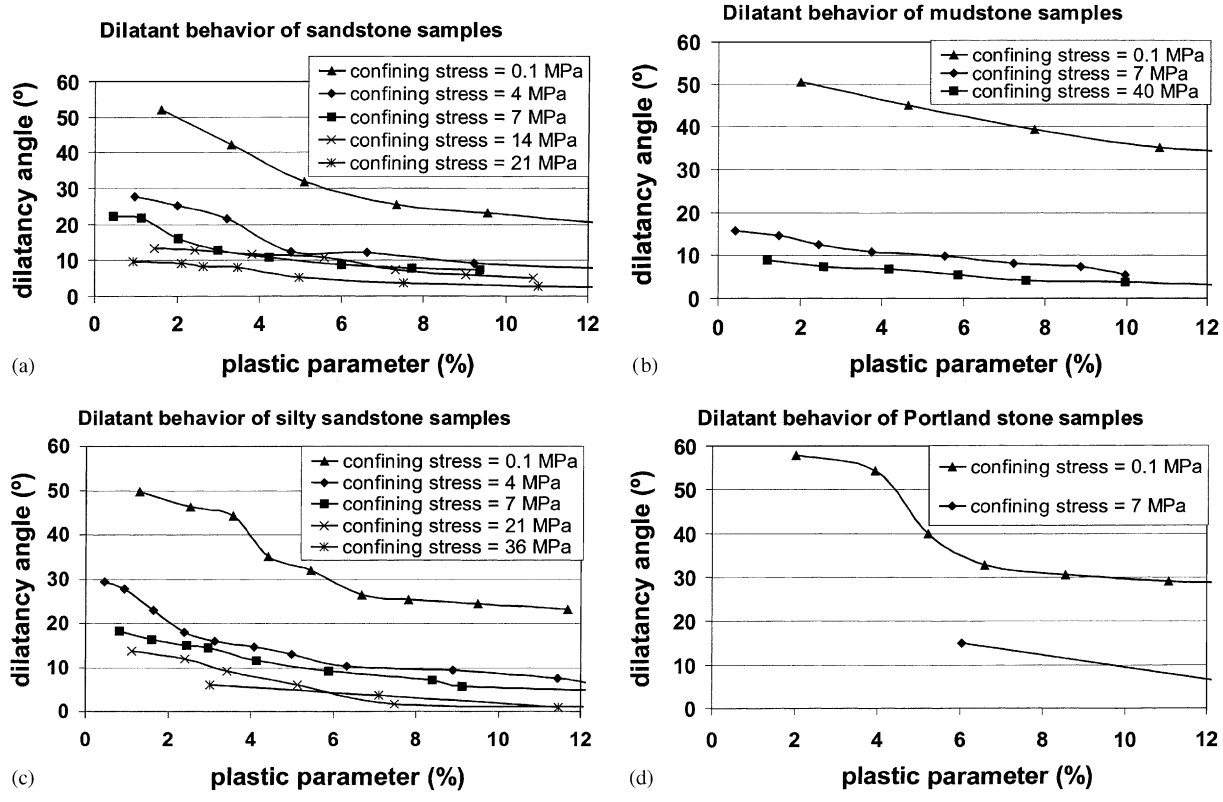

Fig. 7. Dilatancy angle–plastic parameter relationships obtained by reinterpreting four sets of triaxial compressive tests by Farmer [15] performed on standard rock core samples—(a) sandstone, (b) mudstone, (c) silty sandstone, and (d) Portland stone—submitted to different confining stresses.

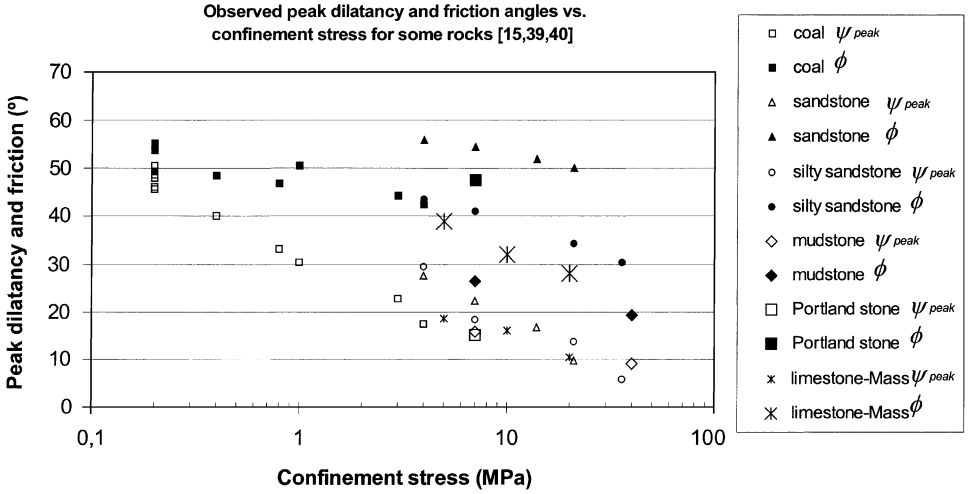

Fig. 8. Peak dilatancy and friction angles, estimated by reinterpreting tests from [15,40] and including data directly estimated by Ribacchi [39].

are less reliable than those for Medhurst's tests, due to the testing procedure, the quality of the graphs from which the values were recovered and the procedure for obtaining plastic strain values. Nonetheless, they do permit us to broaden the framework in which dilatancy is to be analysed.

Fig. 8—in which the estimated peak dilatancy angles and corresponding friction angles are compared to confinement stress—is based on reinterpretation of all the tests and also includes Ribacchi's [39] data. This relatively small database constructed from two sets of tests, combined with the observations of different authors reproduced in Section 3, form the basis for our proposed model for estimating rock dilatancy angles.

5. A dilatancy angle model

The behaviour frame of our model needs the introduction of the elastic parameters. It also needs a softening parameter-dependent failure criterion (i.e. Hoek–Brown or Mohr–Coulmb) as in Eq. (1), in such a way that this failure criterion or their parameters varied from their peak values (for a null value of the softening parameter) to their residual values (for a sufficiently large value of the softening parameter, and where for instance a null cohesion can be included). An example of this failure criterion model was presented by Duncan Fama et al. [32], who introduce an evolving Hoek–Brown failure criterion depending on the plastic shear strain. Another example of this failure criterion model was presented by Alonso et al. [35], who use a Mohr–Coulomb evolving failure criterion, with softening parameter-dependent cohesion and friction (two-segment piece-wise linear functions). The more simple model of this type would be a perfectly plastic model, where the peak, evolving and residual failure criteria coincide. Finally, it is assumed a plastic potential as in Eq. (7), able to accommodate the dilatancy model to be presented.

From a conceptual mechanistic scope, there is justification of the model to be presented in the studies by Archambault et al. [13]. The confining stress dependency has been implemented following a comparison with trend of the phenomena observed by Barton [18,19] and his co-workers for joints. The plasticity dependence reflects the proposal of Detournay [12]. Finally, the model has been adjusted to the results presented by Medhurst [40] and Farmer [15].

In most of the tests analysed above, the dilatancy angle values recovered for very low values of the plasticity parameter were negative or very low. The reason for this is the shape of the complete stress–strain curve, consisting of the initial concave area (due to microfracture and pore closure), the inelastic transversal strain between the onset of stable and unstable fracture propagation, and finally, the hardening stage between this last point and the point of maximum strength (also called short-term compressive strength—see Figs. 2 and 9). These topics are beyond the scope of our proposed formulation, although they could be tracked by the use of more complex models capable of handling heterogeneity [44,45]. Starting from an initial realistic model, the fact that all these inelastic and non-plastic effects are ignored results in an elastic–plastic model capable of including variable dilatancy and strain softening, as depicted in Fig. 9, where a comparison is made with actual observations, and in which the values for peak dilatancy were recovered values and in which the corresponding friction angles were computed from estimated or given Hoek and Brown failure criteria.

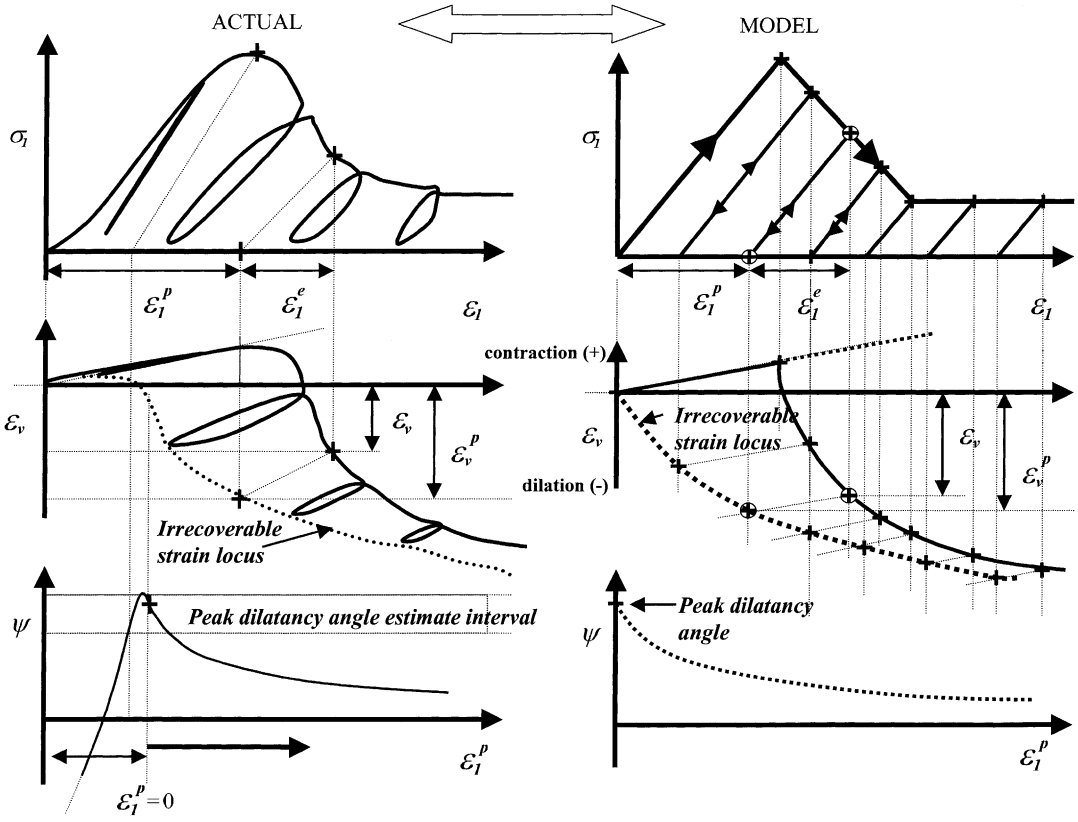

Fig. 9. Actual stress–strain relationships for a compressive test on a strain-softening coal sample with some unloading–loading cycles and ideal stress–strain relations as proposed in our dilatancy model. Reading top to bottom: axial stress vs. axial strain, total and plastic volumetric strain vs. total and plastic axial strain, and the resulting dilatancy angle function.

5.1. The peak dilatancy angle estimate

Since the tests on Moura coal were considered to be more relevant, the peak dilatancy and friction angle values were compared to confinement stress in the first series of tests (Fig. 10a) and to sample diameter in the second series of tests (Fig. 10b). This demonstrates that peak dilatancy is highly dependent on confinement stress but has a limited influence on scale.

In Fig. 8, the estimated peak dilatancy and friction angles for each test are compared to confinement. These were estimated from the slope of the corresponding Hoek and Brown failure criterion for the corresponding stress level and sample size (Fig. 11). Fig. 8 shows how peak dilatancy and friction angles appear to correlate well for low stress levels, whereas for higher stresses the values tend to diverge, with the difference becoming greater as confinement stress increases. It turns out, then, that the assumption $\psi_{\text{peak}} = \phi$ is not an erroneous one for peak dilatancy at very low stress levels, and this would explain the commonplace assumption in regard to associated flow rules in early rock mechanics studies.

Nonetheless, this assumption is clearly imprecise for higher stress levels, as rock failure usually occurs in shear bands or in new discontinuities, and particularly in soft-to-medium rock [15,39,40]. Having recovered the shape of the joint peak dilatancy as per Eq. (22), the following expression is proposed:

$$\psi_{\text{peak}} = ct.\log_{10}\frac{\sigma_{ci}}{\sigma_3} + 0.1, \tag{27}$$

where *ct.* is a constant corresponding to the *JRC* in rock joints, σ_{ci} (MPa) is the intact unconfined compressive strength for rock joint *JCS*, and σ_3 (MPa) is assumed to be equivalent to σ_n. The value 0.1 (MPa) has been added to σ_3 to avoid mathematical problems associated with a null denominator in the logarithm argument for the common case of unconfined stress (a decision that has no effect on the spirit of our approach).

In order to estimate the value of *ct.* we assume—as a consequence of the peak dilatancy value obtained for very low stresses—that it is not inaccurate to consider that $\psi_{\text{peak}} = \phi$ for null confinement pressures ($\sigma_3 = 0$ MPa). The value of *ct.* is thus readily obtainable and can be reintroduced in Eq. (27) to obtain

$$\psi_{\text{peak}} = \frac{\phi}{1 + \log_{10}\sigma_{ci}}\log_{10}\frac{\sigma_{ci}}{\sigma_3 + 0.1}, \tag{28}$$

where ϕ (°) refers to the peak friction angle which can, moreover, be calculated as the slope of the Hoek and Brown failure criterion (Fig. 11). It also includes confinement stress and scale dependencies.

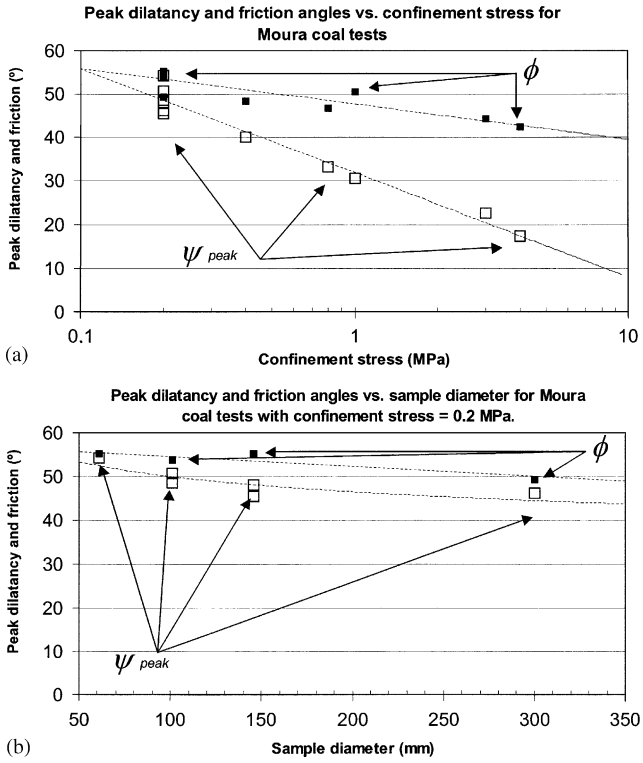

Fig. 10. Peak dilatancy and friction angles obtained from reinterpreting Medhurst's test results [40]: (a) peak dilatancy angle vs. confining stress for a series of triaxial compressive tests on large samples—146 and 300 mm—submitted to different confining stresses between 0.2 and 4 MPa, (b) peak dilatancy angle vs. sample diameter for a series of triaxial compressive tests on different-diameter cylindrical samples submitted to a confinement stress of 0.2 MPa.

The results of applying this formula to the reinterpreted dilatancy angle values for 30 tests are represented in Fig. 12. For 20 tests, error was less than 10% and below 5°; for five tests it was over 50%. The cases corresponding to the higher errors (over 50%) refer to low values of the dilatancy angle (between 0° and 15°). To illustrate the case for instance we have estimated values of 8.3° and 0.7° face to actual values of 15.7° and 9° for mudstone subjected to confinements of 7 and 40 MPa and estimated values of 5.2° and 2° face to actual values of 13.7° and 5.8° for silty sandstone subjected to confinements of 21 and 36 MPa. It is also important to note that these higher errors appear in the less reliable Farmer's data [15]. The authors consider that the fit presented is quite a good one for the case of rock mechanics, where a certain deal of variability can always be expected.

Eq. (28) and the reinterpreted results on which it is partially based are probably not highly accurate, but further fine-tuning would only be possible with a larger and more reliable database. Increased accuracy, moreover, would require a much more complex formula. Nonetheless, as indicated previously, our modelling philosophy is to obtain a suitable trade-off between simplicity and accuracy.

Fig. 10b would also indicate that a further minimal level of scale correction could be introduced in Eq. (28) (some degree of scale correction has already been included via ϕ).

Undoubtedly, the main advantage of Eq. (28) resides in the fact that it permits peak dilatancy angles to be obtained from the most widely available parameters for rocks and rock masses. Even if not highly accurate, it is undoubtedly an improvement over existing techniques.

5.2. Dilatancy angle decay in line with plasticity

In order to study how a dilatancy angle decays as plasticity increases, the first option considered was to assign an exponential decay function for K_ψ or the dilatancy relationship, in such a way that the value of this parameter gradually drops from its initial value, which corresponds to the previously calculated peak value, to a value of one, which corresponds to a zero plastic volume increase. This null value is proposed in the light of the fact that a rock cannot dilate infinitely [7,12]. Although negative values (representing contractions) have been reported for highly porous rocks submitted to very high confinement stress, this is obviously not a very common occurrence [41]. We thus propose:

$$K_\psi = 1 + (K_{\psi,\mathrm{peak}} - 1)\,\mathrm{e}^{-\gamma^{\mathrm{p}}/\gamma^{\mathrm{p},*}}, \tag{29}$$

where the parameter $\gamma^{\mathrm{p},*}$, or plasticity parameter constant, should be calculated for each type of rock; moreover, whether this depends on confinement stress, scale, or the plasticity parameter needs to be investigated. This formulation was chosen for its simplicity; it is based on Detournay [12] and Eq. (19), but also on a study of dilatancy decay in line with plastic parameter growth in the reinterpreted cases (Figs. 5–7).

For our analysis, the values of the plastic parameter were first rescaled, on this occasion for $\gamma^{\mathrm{p}} = 0$; a peak dilatancy angle as defined above and as depicted in the graph in Fig. 9 can be observed. Next, for each reinterpreted test and for each available value for the plastic parameter γ^{p}, the value of $\gamma^{\mathrm{p},*}$ was calculated according to

$$\gamma^{\mathrm{p},*} = -\frac{\gamma^{\mathrm{p}}}{\ln[(K_\psi - 1)/(K_{\psi,\mathrm{peak}} - 1)]}, \tag{30}$$

where $K_{\psi,\mathrm{peak}}$ was taken as observed from the test reinterpretation. Fig. 13, which represents the first series of reinterpreted Moura coal tests, reveals an average value of around 20 mstrain for $\gamma^{\mathrm{p},*}$ and moderate variability. It can also be observed that there is no clear correlation between the value of this parameter and the plasticity parameter or confinement stress.

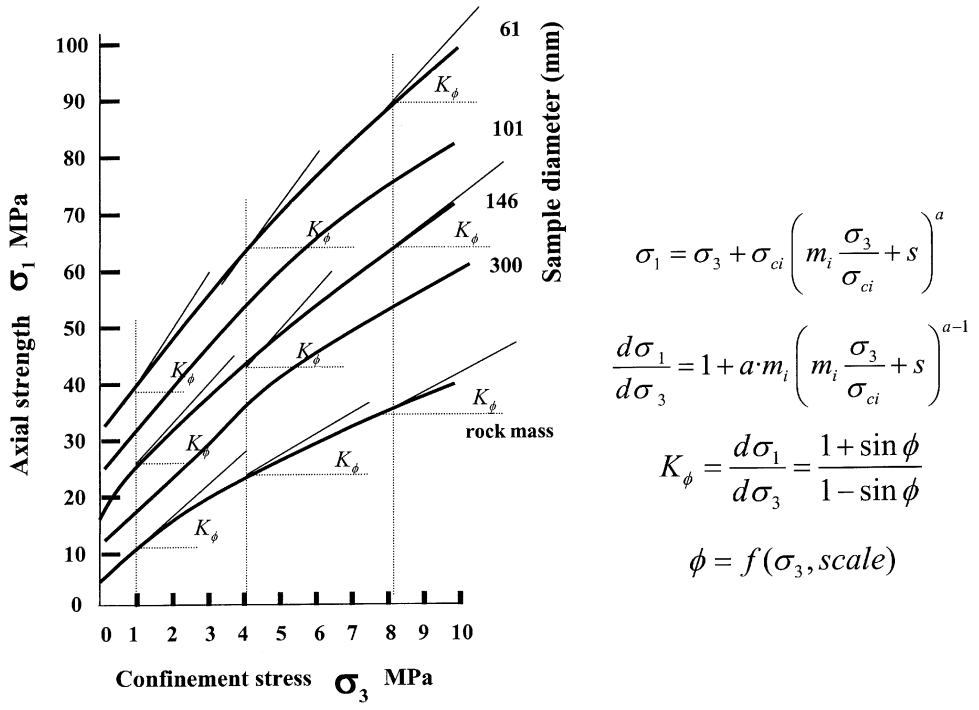

Fig. 11. Peak modified Hoek–Brown failure criteria for samples of Moura coal in a range of diameters (after Medhurst [40]) and the formula for obtaining the friction angle for each sample size and confining stress, showing the dependencies of ϕ on these parameters. *Source*: Adapted from Ref. [40].

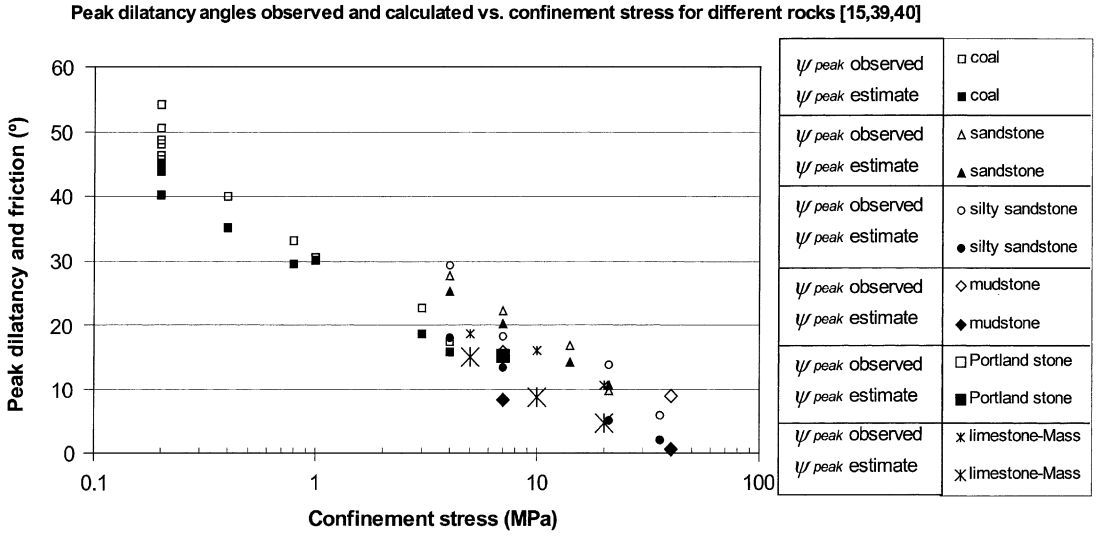

Fig. 12. Reinterpreted peak dilatancy angles as observed in tests from Refs. [15,39,40], and the same values calculated using our dilatancy model.

Once the values for $\gamma^{p,*}$ for all the points recovered from Farmer's tests [15] were compared to the values for γ^p, it could be observed that Eq. (29) was not highly accurate, as $\gamma^{p,*}$ seemed to increase slightly for higher levels of plasticity. However, given the lesser significance of these tests, for the sake of simplicity we have chosen to ignore this fact in our model. To investigate confinement stress dependence further, the values of the relationship $(K_\psi - 1/K_{\psi,\text{peak}} - 1)$ for each Medhurst [40] reinterpreted test and for each plasticity parameter were plotted against confinement stress dependence (Fig. 14). Exponential functions were fitted and show that no clear trends in the relationship $\gamma^{p,*}-\sigma_3$ are evident, an observation which is largely consistent with Farmer's [15] reinterpreted tests.

To study the decay dependency on dilatancy with scale, the relationship $\gamma^{p,*}$—*sample diameter* was plotted from an analysis of the second series of Moura

reinterpreted coal tests; these consisted of six tests submitted to confining stresses of 0.2 MPa on 61, 101, 101, 146, 146 and 300 mm diameter samples. Fig. 15 illustrates a possible tendency for the plasticity parameter constant to decrease in line with scale. Here again, however, the paucity and limited significance of the results would indicate no scale correction.

It should be pointed out that the shape of both relationships, $\gamma^{p,*}$—*sample diameter* (Fig. 15) and ψ_{peak}—*sample diameter* (Fig. 10b), resembles a priori the shape commonly found (in the rock engineering field) when scale effects on parameters such as field stress magnitude, breakdown pressure, elastic modulus and compressive strength are analysed [46], and where the concept of '*Representative Elementary Volume*' is introduced.

As for obtaining a representative value of $\gamma^{p,*}$, Fig. 14 was redrawn as Fig. 16, this time ignoring confining stress in order to estimate a final fit value of $\gamma^{p,*} = 19.7$ mstrain for Moura coal. Similar graphs (Figs. 17a–d) were created for the less reliable Farmer tests in order to obtain the value of this parameter for the different rocks analysed—Moura coal, sandstone, mudstone, silty sandstone and Portland stone. For these five rocks, the

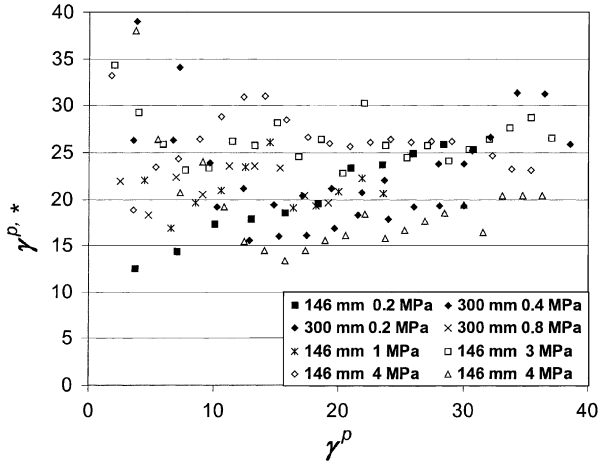

Fig. 13. Estimated values for $\gamma^{p,*}$ for each reinterpreted first Moura coal series tests (compressive tests on large samples—146 and 300 mm—submitted to different confining stresses between 0.2 and 4 MPa) and for every available value of the plastic parameter γ^{p} in the tests.

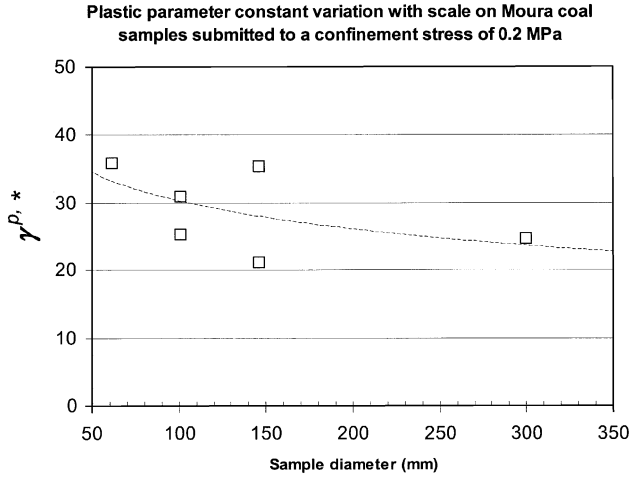

Fig. 15. Estimated relationship between $\gamma^{p,*}$ and sample diameter, resulting from a reinterpretation of the second Moura coal series of tests (six tests on different size samples submitted to confining stresses of 0.2 MPa). This figure illustrates a tendency for the plastic parameter constant to decrease with scale.

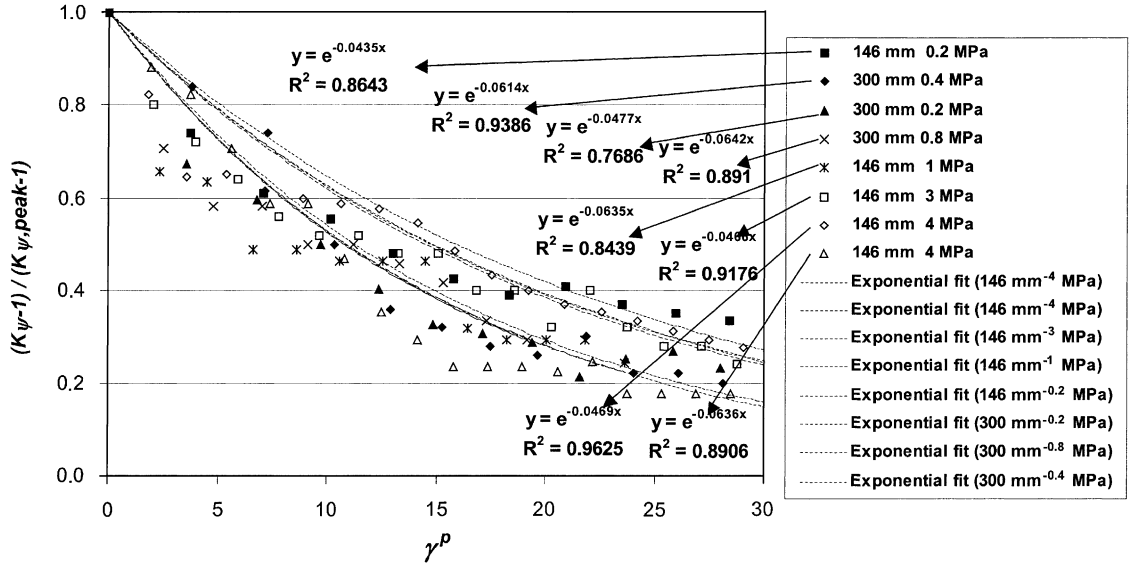

Fig. 14. Estimated values for the relationships $K_{\psi} - 1/K_{\psi,peak} - 1$ vs. γ^{p} for each reinterpreted first Moura coal series test (compressive tests on large samples submitted to confining stresses between 0.2 and 4 MPa), where an exponential function has been fitted to estimate the average value of $\gamma^{p,*}$ for each test. No obvious dependence between $\gamma^{p,*}$ and σ_3 was found.

mean value/standard deviation ratio for the values obtained for $\gamma^{p,*}$ was found to fall between 3 and 4, a value which can be considered eminently useful from a practical rock engineering perspective.

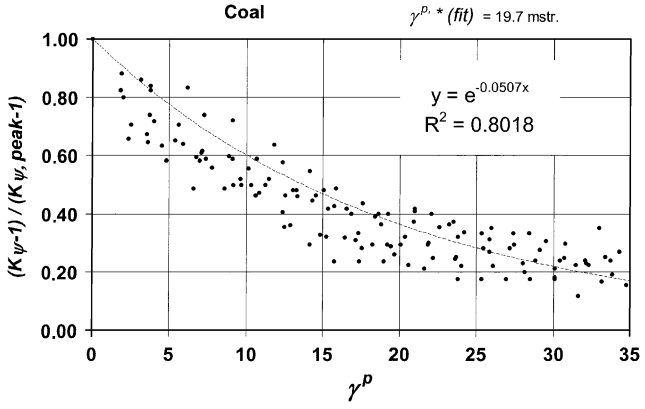

Fig. 16. Representation of Medhurst [40] data in terms of $K_\psi - 1/K_{\psi,\mathrm{peak}} - 1$ vs. γ^{p}. General exponential fit showing an average value of $\gamma^{p,*}$ equal to roughly 20 mstrains for Moura coal.

5.3. Some observations on the dilatancy model

A formula for estimating the dilatancy angle for rock and rock masses is proposed here in accordance with Eqs. (28) and (29). The model incorporates marked dependencies on confining stress and the plasticity parameter, in accordance with observations by other authors. The model also includes an indirect scale effect by means of the inclusion of ϕ in the model. Further scale dependencies were uncovered but were not included in the model, given their lesser significance and the fact that the database was possibly too small and therefore not entirely reliable.

Our approach—like Detournay's [12]—has the advantage that dilatancy is estimated by just a single parameter $\gamma^{p,*}$, yet takes into account scale effects and confinement stress dependency. Modellers, therefore, need to include in their inputs, a reasonable approximation of this parameter rather than a more or less unrealistic constant value for the dilatancy angle.

Fig. 18, which illustrates the application of the model to the reinterpreted first series of Moura coal tests,

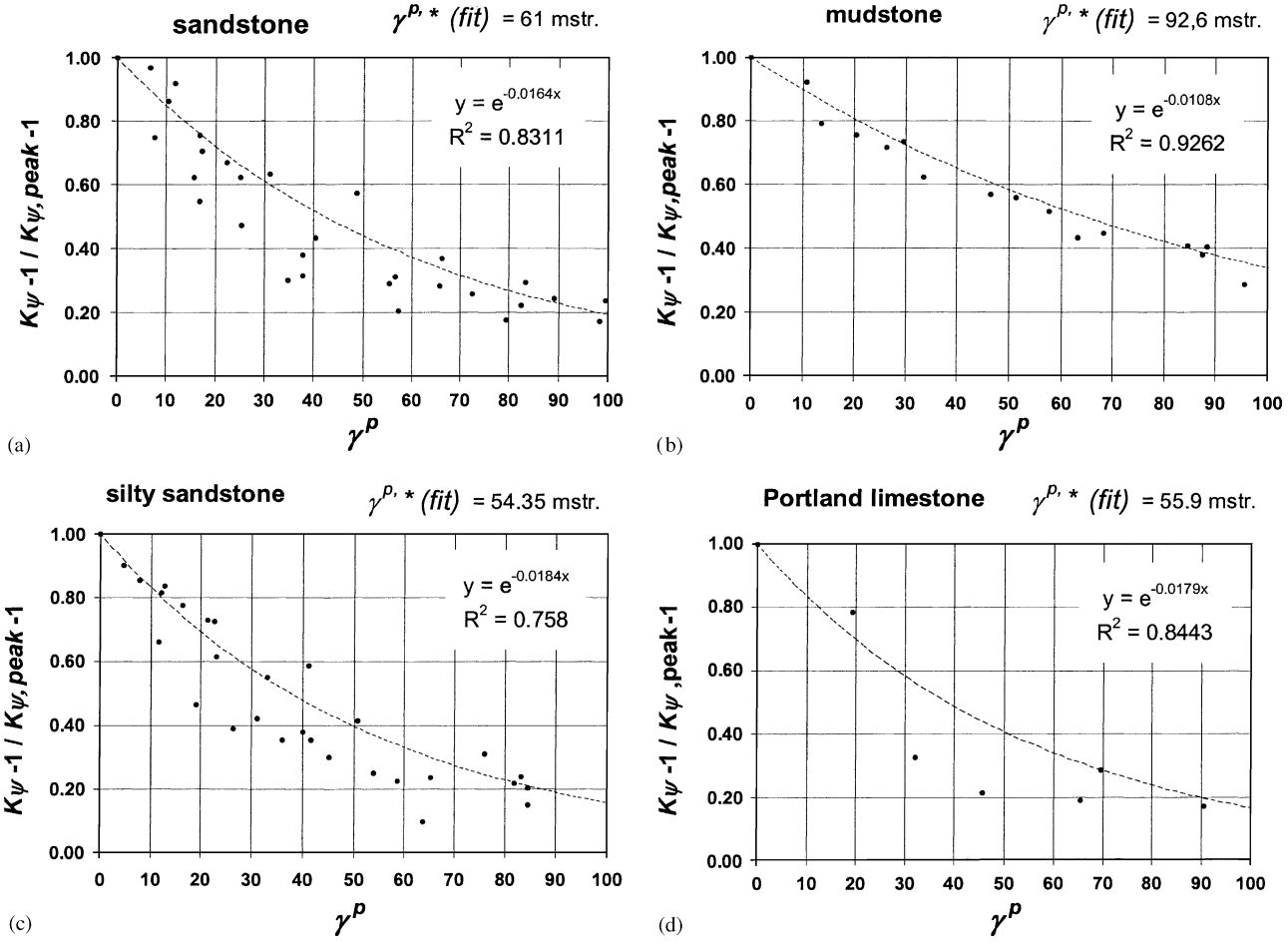

Fig. 17. Representation of Farmer data [15] for the tests on different rocks—(a) sandstone, (b) mudstone, (c) silty sandstone, and (d) Portland stone)—reinterpreted in terms of $K_\psi - 1/K_{\psi,\mathrm{peak}} - 1$ vs. γ^{p}. Corresponding exponential fits, showing the estimated values for the constant $\gamma^{p,*}$ for each type of rock.

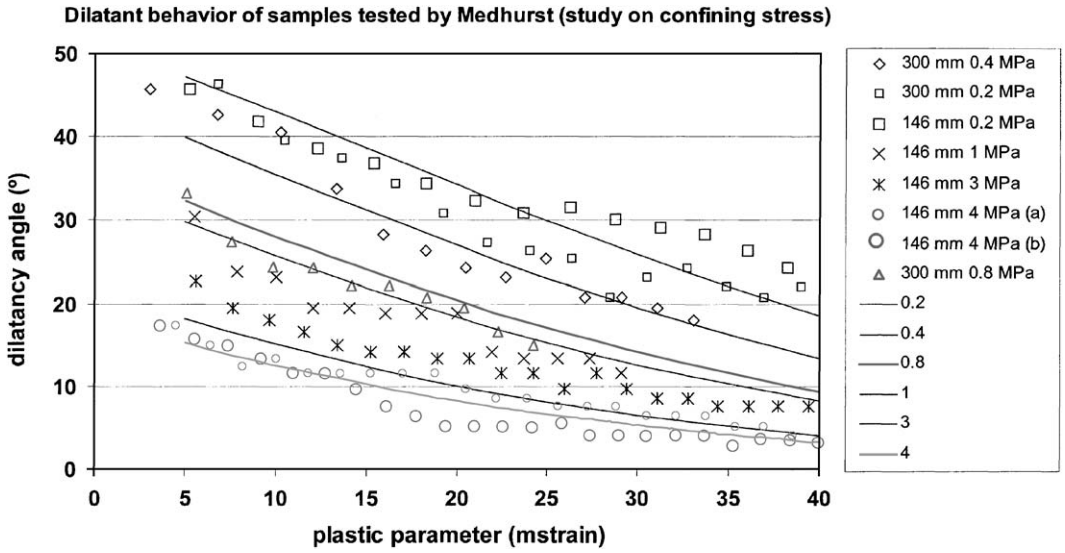

Fig. 18. Observed (reinterpreted from tests) and estimated (according to our dilatancy model) relationship between the dilatancy angle and the plastic parameter for the first Medhurst [40] series of triaxial compressive tests on large samples—146 and 300 mm—submitted to confining stresses of 0.2, 0.2, 0.4, 0.8, 1, 3, 4 and 4 MPa.

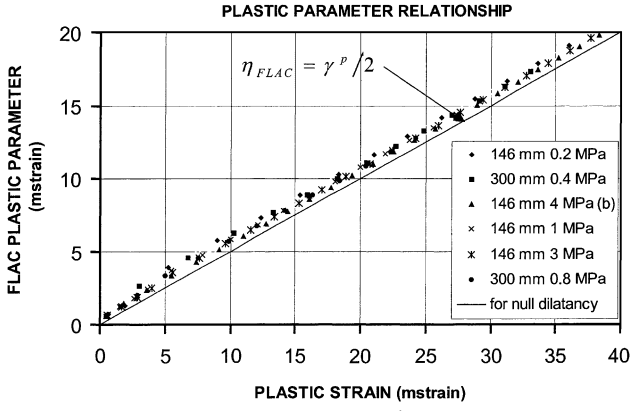

Fig. 19. For some of the Medhurst [40] reanalysed tests, relationship between the FLAC [26] plastic parameter e^{ps} and the more standard plastic parameter represented by the plastic shear strain $\gamma^p = \varepsilon_1^p - \varepsilon_3^p$ for the simple case of null dilatancy.

includes the original results together with the fit of the model. Starting from $\gamma^p = 5$ mstrain—to cope with the non-elastic and non-plastic effects—the result is a satisfactory level of agreement.

One of the aims of this study was to present a model that could be easily implemented in numerical codes. To facilitate the application of this dilatancy model in a code as widely used as FLAC, a relationship needs to be established between the plastic parameters γ^p and e^{ps}. For null dilatancy it has been shown that e^{ps} is twice γ^p, a ratio that can be maintained for the general case without inducing significant error. Fig. 19 shows how this relationship evolves over different deformation stages for some of the reinterpreted tests. Eq. (29) can thus be easily converted into

$$K_\psi = 1 + (K_{\psi,\text{peak}} - 1)\, e^{-e^{ps}/e^{ps,*}}. \tag{31}$$

In Eq. (31) the new plasticity parameter constant is related to the previous value in accordance with

$$e^{ps,*} = \frac{\gamma^{p,*}}{2}. \tag{32}$$

Once this relationship is known, it is a simple matter to create a subroutine in which to implement the formulation for use in a commercial code like FLAC.

Although the proposed dilatancy model does not require the inclusion of strain softening, such a model would be useful from the perspective of including all possible post-failure strength modes, from elastic–perfectly plastic to purely brittle.

6. Sample applications

In this section, the proposed dilatancy model is applied to two problems where dilatancy is known to play a significant role. Results are compared to actual test results and to relevant observations on the behaviour of rock masses. Note that these can only be considered preliminary results, as more research would be required to better calibrate the range of the model; nonetheless, they will serve to demonstrate the model's potential.

6.1. Application to servo-controlled tests modelled using FLAC-2D

FLAC-2D [26] was used to model the servo-controlled triaxial compression tests of a Mohr–Coulomb

strain-softening material representing Moura coal. The peak and residual Mohr–Coulomb failure criteria were estimated for 300 mm diameter samples from proposed [40] peak and residual Hoek and Brown failure criteria. For each confining level the evolving values of the failure criteria estimated from test results were obtained. Used for the sake of simplicity were simple cohesion and friction bilinear decay functions (as proposed in [35]), adjusted to the test results. The elastic parameters, Young's modulus and Poisson's ratio used initially were those recovered from the tests. A standard servo-control function was used to minimize the influence of inertial effects on model response. Created for this application was a subroutine to implement our dilatancy angle model in the FLAC code, written in FLAC's internal language FISH.

First modelled were three servo-controlled tests on 300 mm cylindrical coal samples (the axisymmetric option) submitted to confinement stresses of 0.2, 0.8 and 4 MPa. A square 15 mm grid size has been used. The total volumetric strain–total axial strain results presented in Fig. 20a together with analogous results from actual tests reveal moderately good agreement. The observable offset between model and actual data (the

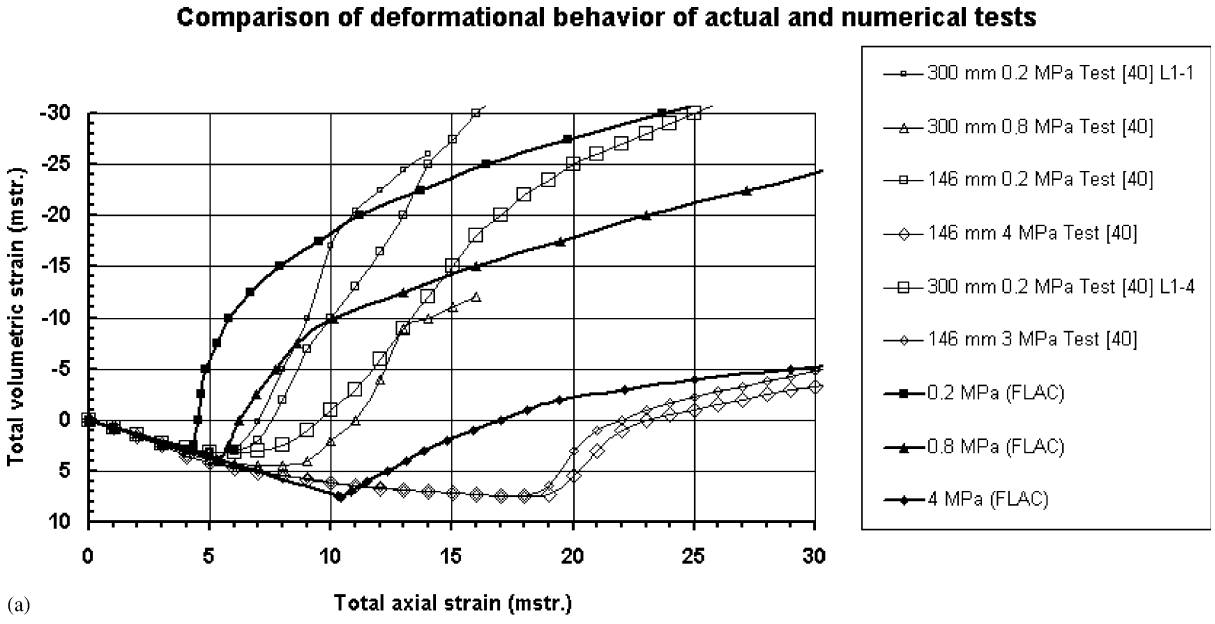

(a)

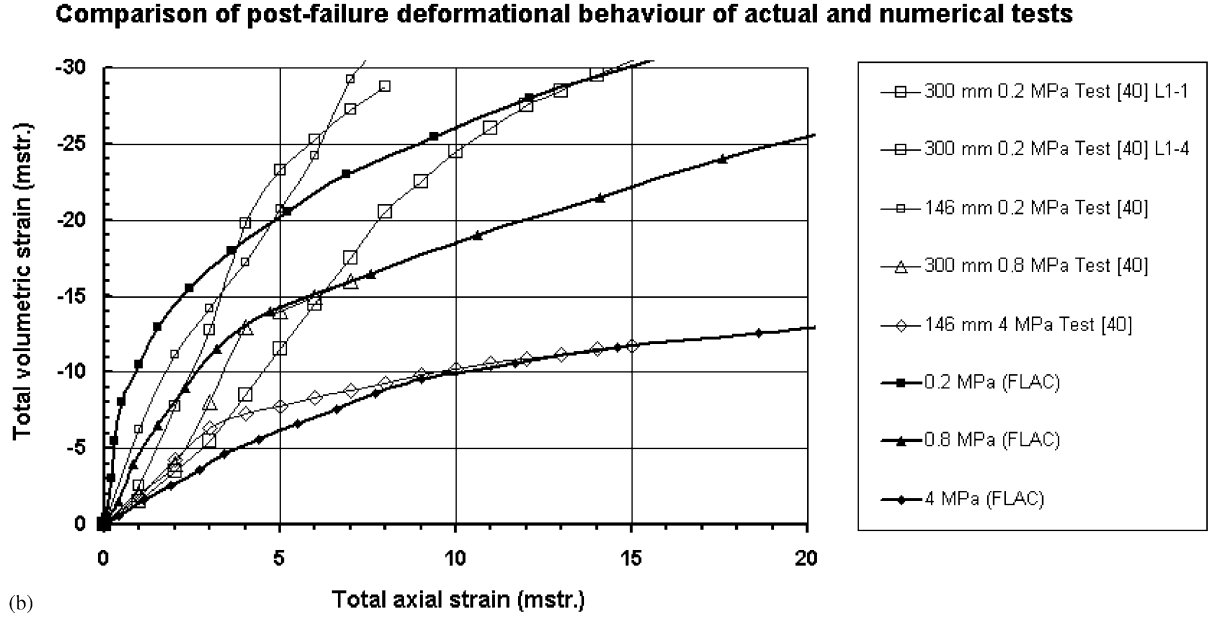

(b)

Fig. 20. (a) Volumetric–axial strain curves for compressive triaxial tests on cylindrical coal samples submitted to low, medium and high confining stress. Actual results as recovered from Medhurst [40] and results computed using code FLAC [26] using our dilatancy model and the actual values of the tangent Young's modulus back-calculated from tests. (b) Corrected post-failure volumetric–axial strain curves for the tests presented in (a).

model data is moved to the left-hand side) is due to the fact that the model is incapable of representing the damage or behaviour of the rock between long- and short-term strengths in the pre-failure deformation stages; this increases the level of plastic axial strain and, in turn, total axial strain, an effect which could be overcome by implementing degradation models in the code [45]. Fig. 20b illustrates post-failure deformational behaviour for the same tests; strain values were corrected to represent the values starting from the point corresponding to maximum strength. In this figure, a better fit can be observed. Note that there is a moderate degree of variability in the actual tests, so it would, in fact, be difficult to define a good fit.

In order to avoid any inaccuracies arising from the use of the tangent Young's modulus, secant Young's modulus was estimated from the tests and subsequently adjusted. In order to reflect the deformational behaviour shown in Fig. 21—where a reasonable agreement is observed—the initial models corresponding to 0.2, 0.8 and 4 MPa were recreated. In order to assess the effects of mesh size, three different grid sizes were modelled for each confining stress.

Mesh size was observed to be of little significance (a peak strength variation of less than 5%), except when very small, when bifurcation and localization phenomena were likely to occur. However, it is a topic for further research together with scale effects. Note also that any numerical problems related to grid size would be attenuated in rock mass models.

These examples serve to show that the outputs given by our approach are able to reasonably represent the behaviour observed on coal specimens. Further examples under different conditions and for different rocks are needed in order to fully validate the dilatancy model.

6.2. Application to ground reaction curves for tunnel design

The dilatancy model described above was used to obtain ground reaction curves. These curves, which form the basis for the convergence-confinement method, are widely used in tunnel design. This analysis permits an association between convergence in the wall and the formation of a plastic aureole around a tunnel of radius R under a hydrostatic field stress of magnitude σ^0, to the value of an internal pressure initially equal to the field stress, which is diminished to a null value and which can be related to the distance from the face [47,48]. This simple analysis is often used as a point of departure for studying the mechanics of deformation in underground excavations [49].

Analytical solutions exist for simple cases of ground reaction curves for circular tunnels excavated in elastic, perfectly plastic [47], brittle [50] Mohr–Coulomb media, as also in elastic, perfectly plastic, standard and modified Hoek and Brown rock masses [51,52]. A numerical self-similar solution also exists for the case of strain-softening continua [35], based on the suitable definition of a fictitious 'time' variable and the rescaling of certain variables. This converts the problem into an initial-value problem that can be solved numerically using the Runge–Kutta–Fehlberg method [53] as implemented in a MATLAB environment. We chose this solution for implementing our dilatancy formula, as it

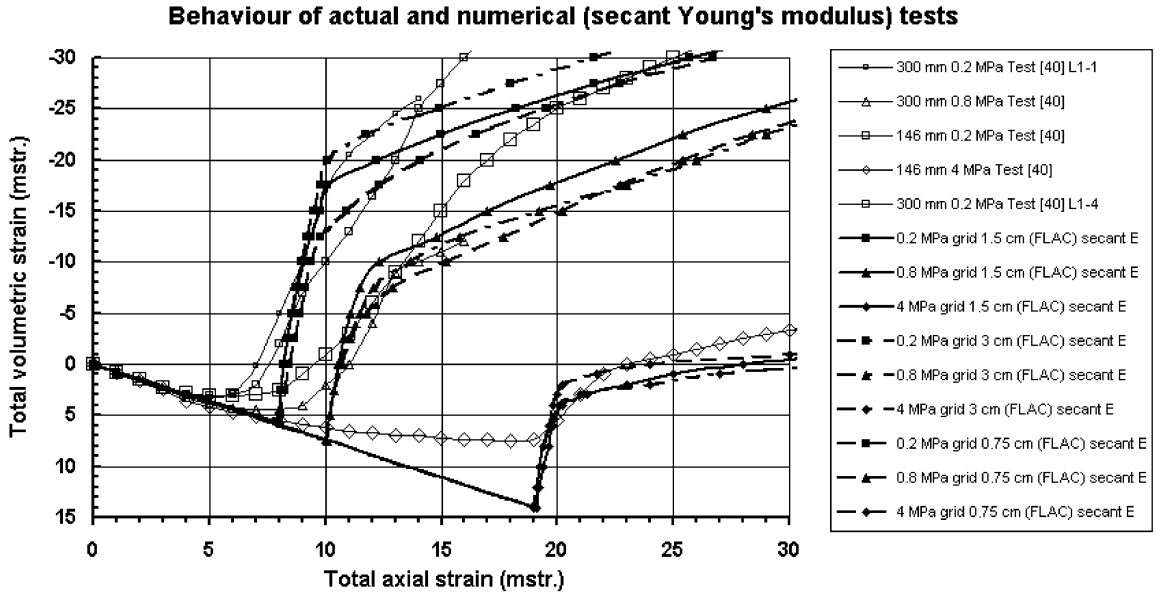

Fig. 21. Volumetric–axial strain curves for compressive triaxial tests on cylindrical coal samples submitted to low, medium and high confining stress. Actual results as recovered from Medhurst [40] and results computed using code FLAC [26] using our dilatancy model and the actual values of the secant Young's modulus back-calculated from test results.

permits variable dilatancy to be included. Using this approach, we were able to compute ground reaction curves for tunnels excavated in strain-softening continua with confinement stress and plasticity-dependent dilatancy. Other numerical techniques based on FDM or FEM codes can be also used to apply the model. With a view to assessing average dilatancy values and studying how these evolve in excavation processes, the next section describes a simulation of two rock masses.

6.2.1. Case 1. A perfectly plastic rock mass

From a standard poor-quality and perfectly plastic rock mass, a set of suitable parameters were estimated using RocLab [54] (for $GSI = 18$, $\sigma_{ci} = 20\,\text{MPa}$ and $m_i = 9$). Elastic parameters were $G = 700\,\text{MPa}$ (shear modulus) and $v = 0.3$ (Poisson's ratio), and strength parameters were cohesion $= 0.5\,\text{MPa}$ and $\phi = 20^\circ$. The required value for $\gamma^{p,*}$ for the dilatancy model was fixed at 100 mstrain, similar to that obtained for mudstone.

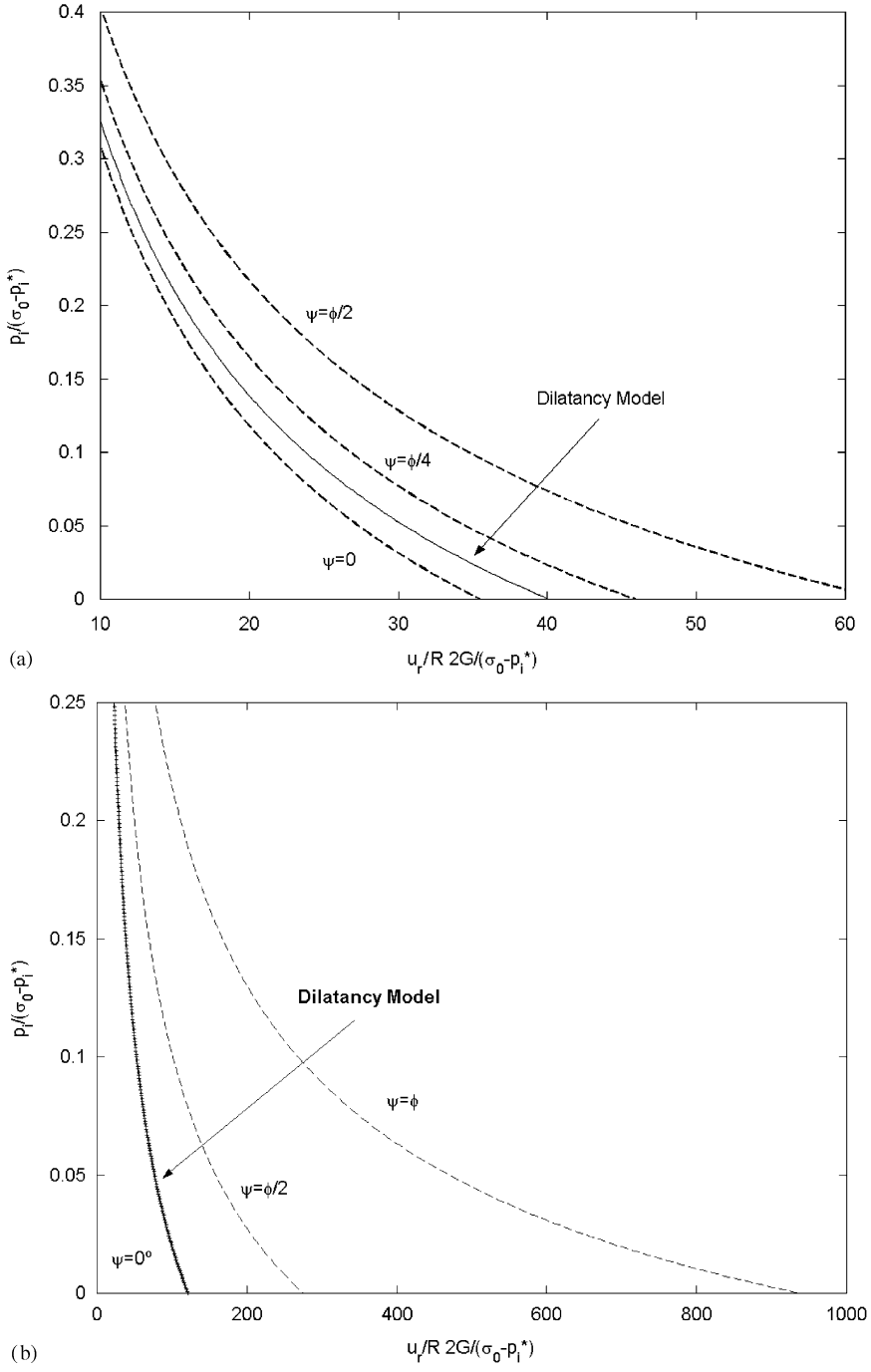

Fig. 22. Normalized ground reaction curves for perfectly elasto-plastic rock mass, obtained using our dilatancy model and using a constant dilatancy value. The two curves correspond to isotropic field stresses of (a) 10, and (b) 20 MPa (p_i^* is the internal pressure that indicates the elastic–plastic transition).

A tunnel of radius R was excavated in this rock mass for field stresses equal to 10 MPa (roughly 400 m deep) and 20 MPa (roughly 800 m deep).

The normalized ground reaction curves obtained for the tunnels in the variable dilatancy rock mass are depicted in Figs. 22a and b for the above-mentioned field stresses, together with the curves for significant constant dilatancy cases. It can be observed how the ground reaction curves are very close to those for null dilatancy, most particularly the curves for the higher field stresses. The dilatancy angle values in a radial direction—from the elastic–plastic boundary to the tunnel wall—for the end of the unloading process are represented in Figs. 23a and b in terms of the plasticity

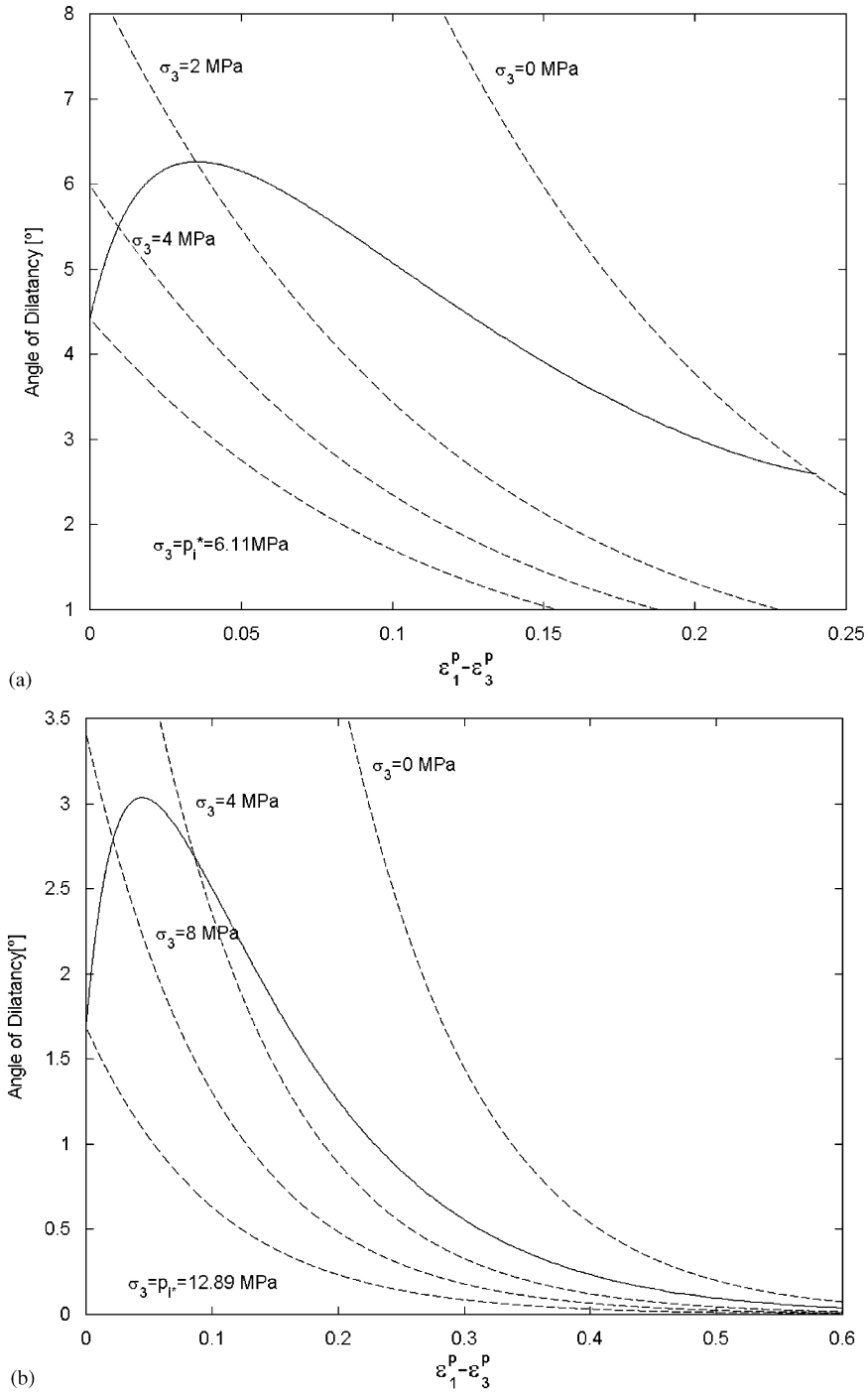

Fig. 23. Evolution of the dilatancy angle value at the boundary of the excavations along the tunnel unloading process (solid line) according to our dilatancy model, for elasto-plastic rock mass and including isotropic field stresses of (a) 10, and (b) 20 MPa (corresponding to the ground reaction curves in Fig. 22). The decaying dilatancy curves for different values of confinement stress are shown by dotted lines.

parameter, together with the corresponding general dilatancy models for confinement stress (to the point at which the plasticity parameter stops increasing). Self-similarity in the problem means that this graph also represents the evolution of the dilatancy angle at a point located very close to the tunnel wall. Both figures show average dilatancy angle values within a range of 3–6° for $\sigma^0 = 10$ MPa, and within a range of 0–3° for $\sigma_0 = 20$ MPa. From these results and from the proposed general model, it is clear that actual dilatancy angle values are not only dependent on the quality of the rock mass, but also on the stress to which the excavation is initially submitted. The constant dilatancy angle values needed to obtain ground reaction curves such as those produced by our model are quite close to the $\psi = 0°$ indicated by Hoek and Brown [20] for this kind of rock mass.

6.2.2. Case 2. A strain-softening rock mass

A rock mass representing the standard Moura coal rock mass, as described by Medhurst [40], was considered together with a set of suitable parameters, which were estimated according to Medhurst's method and using the reinterpreted tests described in Section 4. Elastic parameters were chosen as $G = 2000$ MPa and $v = 0.26$. Peak strength parameters were cohesion = 1.2 MPa and $\phi = 37°$, and residual strength parameters (approximate estimates by the authors) were cohesion = 0.6 MPa and $\phi = 20.6°$. The strength decay parameter required to model the evolving failure criteria was assumed to be bilinear decaying from peak at 0 mstrain to residual at approximately 15 mstrain [35], with $\sigma_{ci} = 32.7$ MPa and $\gamma^{p,*} = 20$ mstrain. A tunnel of radius R was excavated in the coal rock mass for field stresses equal to 10 and 20 MPa.

The normalized ground reaction curves obtained are depicted in Fig. 24, together with the curves for selected constant dilatancy cases. These curves, which take variable dilatancy into account, closely approximate the curves for a dilatancy value equal to $\phi/8$, as indicated by Hoek and Brown [20] for average-quality strain-softening rock masses. The curves for a field stress of 10 MPa (Fig. 24a) and for a field stress of 20 MPa (Fig. 24a) lie, respectively, just above and below the curve corresponding to a dilatancy value of $\phi/8$.

The final dilatancy values for both cases—represented in Fig. 25—show an average (somewhat surprising) value of around 15° for 10 MPa (Fig. 25a) and a more predictable range of values between 0° and 10° for 20 MPa (Fig. 25b). The ψ value of around 15° for the former is due to the low plasticity values obtained; the dilatancy angle does not have sufficient space to attenuate because the plasticity parameter is still low when the unloading process finishes, so a kind of "brittle" behaviour appears in the annulus of plastic or yielding rock. This fact might contribute to explain the use of early support in tunnels.

6.3. Final comments

The applications described above were chosen for their usefulness in highlighting some interesting rock mechanics issues and showing how the dilatancy problem can be handled and understood using a confinement stress and plasticity-dependent model. Other possible applications of this model include studies of mine pillars, coal drifts near long-walls, and tunnel faces in soft rocks.

The axisymmetric model of compressive tests described above has demonstrated how our dilatancy model could be useful for simulating the actual behaviour of rock samples. However, degradation should be incorporated in the model in some way in order to fine-tune results [44,45].

We have shown how, for poor-quality rock mass tunnels, ground reaction curves coincide almost exactly with null dilatancy curves. We have also shown how the average dilatancy values for average-quality coal masses approach the values proposed by Hoek and Brown [20]. In both cases analysed above, therefore, the Hoek and Brown [20] proposal concerning dilatancy (as discussed in Section 3.3 above) makes complete sense, and is, moreover, entirely compatible with Detournay's [12] statements on the nature of dilatancy.

An adequate treatment of dilatancy is crucial to the correct modelling of underground excavation behaviour, irrespective of whether use is made of analytical or pseudo-analytical techniques (e.g. ground reaction curves) or numerical models. Dilatancy stress dependence may also play a significant role in assessing the effectiveness of early support or in shedding some light on the effects of reinforcement on already yielding rock masses.

Ground reaction curves are sometimes linked to the New Austrian Tunnelling Method (NATM) which, although very useful in general, has revealed itself to have certain drawbacks in some excavations carried out using the method [55]. Gaining a solid reputation, on the other hand, as a full-fledged, almost infallible but somewhat expensive tunnelling technique, is the New Italian Tunnelling Method, or ADECO/SR (analysis of controlled deformation in rocks and soils) [56]. If the NATM partially relies on ground reaction curves, when using the ADECO/SR method it is highly appropriate to make models that will predict deformations in the tunnel front (and yielding in the core), for which purpose, Lombardi's method [57] or similar numerical techniques can be used. In order to reliably apply these methods, a better knowledge of actual dilatancy angle values—obtained, e.g. using the model described here—would be highly valuable.

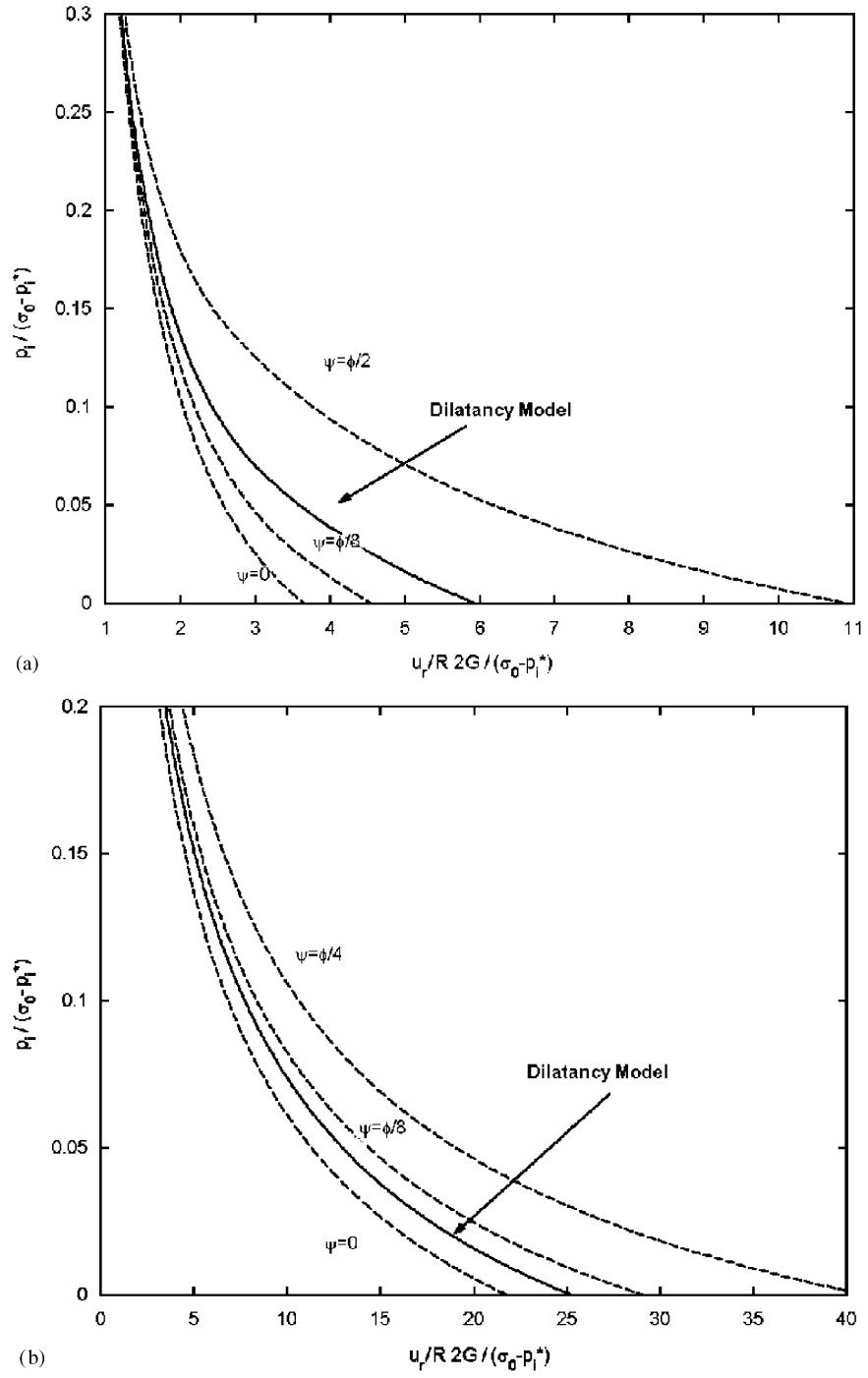

Fig. 24. Normalized ground reaction curves for the coal strain-softening rock mass, for different levels of dilatancy and including two cases for isotropic field stresses of (a) 10, and (b) 20 MPa, obtained using our dilatancy model.

The dilatancy model presented has no universal validity, so it should be used carefully. Hence, it is not appropriate to model stratified rock masses—specially with narrow strata and low-strength bedding planes. In this case the bedding strata behaviour should be included in the model explicitly or by means of the so-called ubiquitous joint model. It is recommended to use this dilatancy model within the frame of wider modelling strategy as proposed by Starfield and Cundall [9].

7. Conclusions

This paper has described a new model to estimate the dilatancy angle in rocks and rock masses. Our starting point was a review of classic definitions of dilatancy angle, a review of early and recent studies dealing with dilatant behaviour in rock, rock joints and rock masses and, finally, a reinterpretation of previously published compressive test results for a range of rocks. Our model

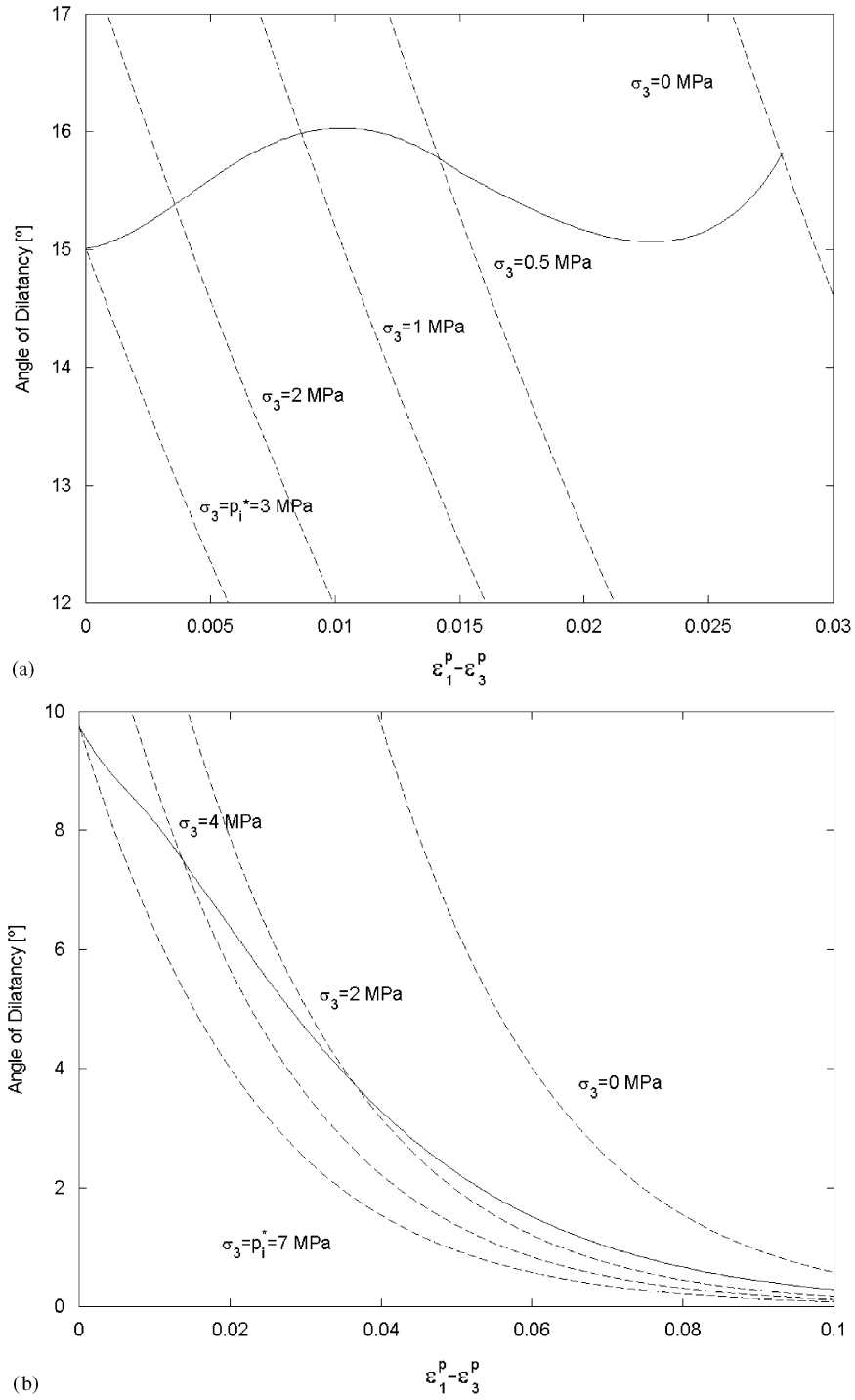

Fig. 25. Evolution of the dilatancy angle value at the boundary of the excavations along the tunnel unloading process (solid line) according to our dilatancy model, for elasto-plastic rock mass and including isotropic field stresses of (a) 10, and (b) 20 MPa (corresponding to the ground reaction curves in Fig. 24). The decaying dilatancy curves for different values of confinement stress are shown by dotted lines.

reflects dependencies on confining stress, on the plasticity suffered by the material and indirectly on scale. Further scale dependencies are speculated on, although not included in the model due to both the lack of sufficient and reliable data and the need to balance simplicity and accuracy. Comparison of model results with actual test data shows moderately good agreement.

The two main advantages of the model are that, first of all, it does not increase the number of parameters needed to model either a rock or rock mass, and secondly, that it can be easily implemented in standard numerical models.

Our dilatancy model was applied to some typical rock mechanics post-failure problems. It was used, first of all,

to axisymmetrically model compressive triaxial tests on cylindrical rock samples. The model produced good agreement with actual test results (the main deformational behavioural trends were successfully captured), which can be considered to numerically validate the method. Secondly, the dilatancy model was used to obtain ground reaction curves for tunnels in poor- and average-quality rock masses, resulting in dilatancy values that correlated well with observations based on wide experience in practical rock engineering.

Our model is potentially useful for understanding the valuable role played by early support in the form of shotcrete, as also for studying the stabilizing effects of reinforcement in yielding rock masses. The model can also make reasonable predictions of deformations in a tunnel face, which is particularly useful in view of more recent approaches to tunnelling design and construction. These are all topics that will be addressed in future research by the authors.

Finally, of undoubted significance is the fact that this approach to obtaining the dilatancy angle is consistent with most of the previously published observations on the subject. Moreover, as our examples demonstrate, the model appears to be capable of tracking actual behaviour and confirming certain rules-of-thumb applied in engineering practice. Above all, it is a relatively simple model to apply, and can be used in conjunction with modelling tools that are widely used in the rock mechanics discipline.

Acknowledgements

The authors thank the local government of Galicia (Xunta de Galicia), Spain, for financial support of the research project entitled 'Obtaining Ground Reaction Curves of Excavations in Rock Masses', under contract reference number (PGIDT03PXIB30401PR).

References

[1] Hudson JA, Brown ET, Fairhurst C. Shape of the complete stress–strain curve for rock. Proceedings of the 13th Symposium on Rock Mechanics, University of Illinois, 1971.
[2] Jaeger JC, Cook NGW. Fundamentals of rock mechanics. 2nd ed. Norwich: Science Paperbacks; 1976.
[3] Price AM, Farmer IW. Application of yield models to rock. Int. J. Rock Mech. Min. Sci. Geomech. Abstr. 1979;16:157–9.
[4] Brace WF, Paulding BW, Scholz C. Dilatancy in the fracture of crystalline rock. J. Geophys. Res. 1966;71(16):3939–53.
[5] Cook NGW. An experiment showing that dilatancy is a pervasive volumetric property of brittle rock loaded to failure. Rock Mech. 1970;2:181–8.
[6] Moss WC, Gupta YM. A constitutive model describing dilatancy and cracking in brittle rocks. J. Geophys. Res. 1982;81(B4):2985–98.
[7] Vermeer PA, de Borst R. Non associated plasticity for soils, concrete and rock. Heron 1984;29(3):3–64.
[8] Elliot GM, Brown ET. Further development of a plasticity approach to yield in porous rocks. Int. J. Rock Mech. Sci. Geomech. Abstr. 1986;23:151–6.
[9] Starfield AM, Cundall PA. Towards a methodology for rock mechanics modelling. Int. J. Rock Mech. Sci. Geomech. Abstr. 1988;25(3):99–106.
[10] Kudoh K, Koyama T, Nambo S. Support design of a large underground cavern considering strain-softening of the rock. 9th ISRM Congress, Paris, vol. 1. Balkema: Rotterdam; 1999 (p. 407–411).
[11] Alejano LR, García Bastante F, Alonso E, Taboada J. Back-analysis of a rock-burst in a shallow room and pillar gypsum exploitation. 9th ISRM Congress, Paris, vol. 2. Rotterdam: Balkema; 1999 (p. 1077–1080).
[12] Detournay E. Elasto-plastic model of a deep tunnel for a rock with variable dilatancy. Rock Mech. Rock Eng. 1986;19:99–108.
[13] Archambault G, Roleau A, Daigneault R, Flamand R. Progressive failure of rock masses by a self similar anastomosing process of rupture at all scales and its scale effects on their shear strength. In: Pinto da Cunha, editor. Proceedings of the Second International Workshop on Scale Effects in Rock Masses, Lisbon. Rotterdam: Balkema; 1993. p. 133–41.
[14] Shih-Che Yuan, Harrison JP. An empirical dilatancy index for the dilatant deformation of rock. Int. J. Rock Mech. Sci. 2004;41: 679–86.
[15] Farmer IW. Engineering behaviour of rocks. 2nd ed. London: Chapman & Hall; 1993.
[16] Medhurst TP, Brown ET. A study of the mechanical behavior of coal for pillar design. Int. J. Rock Mech. Sci. Geomech. Abstr. 1998;35(8):1087–105.
[17] Sterpi D. An analysis of geotechnical problems involving strain-softening effects. Int. J. Numer. Anal. Meth. Geomech. 1999;23:1427–54.
[18] Barton N, Choubey V. The shear strength of rock joints in theory and practice. Rock Mech. 1977;1 & 2:1–54.
[19] Barton N, Bandis SC. Effects of block size on the shear behaviour of jointed rocks. 23rd US Sympsium on Rock Mechanic, vol. 10. Rotterdam: Balkema; 1982 (p. 739–760).
[20] Hoek E, Brown ET. Practical estimates of rock mass strength. Int. J. Rock Mech. Sci. Geomech. Abstr. 1997;34(8):1165–87.
[21] Duncan Fama ME. Numerical modelling of yield zones in weak rock. In: Hudson J, editor. Comprehensive rock engineering, vol. 2. Oxford: Pergamon Press; 1993. p. 49–75.
[22] Gutierrez M. Shear band formation in rocks with a curved failure surface. Int. J. Rock Mech. Min. Sci. 1998;35(4–5) (paper no. 95).
[23] Hill R. The mathematical theory of plasticity. Oxford: Oxford University Press; 1950.
[24] Lubliner J. Plasticity theory. New York: McMillan; 1990.
[25] Kaliszky S. Plasticity: theory and engineering applications. Amsterdam: Elsevier; 1989.
[26] ITASCA. User manual for FLAC, Version 4.0. Minnesota: Itasca Consulting Group, Inc.; 2000.
[27] Drucker DC. A definition of stable inelastic material. J. Appl. Mech. 1959;26(1):101–6.
[28] Cividini A. Constitutive behaviour and numerical modelling. In: Hudson J, editor. Comprehensive rock engineering, vol. 1. Oxford: Pergamon Press; 1993. p. 395–426.
[29] Read HE, Hegemeier GA. Strain softening of rock, soil and concrete—a review article. Mech. Mater. 1984;3:271–94.
[30] Sture S, Ko HY. Strain-softening of brittle geologic materials. Int. J. Numer. Anal. Meth. Geomech. 1978;2:237–53.
[31] Vardoulakis IG, Sulem J. Application of bifurcation theory of rock mechanics problems. In: Hudson J, editor. Comprehensive rock engineering, vol. 1. Oxford: Pergamon Press; 1993. p. 575–610.

[32] Duncan Fama ME, Trueman R, Craig MS. Two and three dimensional elastoplastic analysis for coal pillar design and its application to Highwall-mining. Int. J. Rock Mech. Sci. Geomech. Abstr. 1995;32(3):215–25.
[33] Muir Wood AD. Soil behaviour and critical state soil mechanics. Cambridge: University Press; 1990.
[34] Graham J, Noonan ML, Lew KV. Yield states and stress–strain relationships in a natural plastic clay. Can. Geotech. J. 1983; 20(3):502–16.
[35] Alonso E, Alejano LR, Varas F, Fdez-Manin G, Carranza-Torres C. Ground Reaction Curves for tunnels in strain-softening rock masses. Int. J. Numer. Anal. Meth. Geomech. 2003;27:1153–85.
[36] Drescher A, Vardoulakis I. Geometric softening in triaxial tests on granular material. Geotechnique 1982;32(4):291–303.
[37] Scholz CH. Micro-fracturing and the inelastic deformation of rock in compression. J. Geophys. Res. 1968;73:1417–32.
[38] Brown ET, Bray JW, Ladanyi B, Hoek E. Ground response curves for rock tunnels. J. Geotech. Eng. 1983;109(1):15–39.
[39] Ribacchi R. Mechanical tests on pervasively jointed rock material: insight into rock mass behaviour. Rock Mech. Rock Eng. 2000;33(4):243–66.
[40] Medhurst TP. Estimation of the in situ strength and deformability of coal for engineering design. PhD thesis, University of Queensland, Australia, 1996.
[41] Besuèlles P, Desrues J, Raynaud P. Experimental characterization of the localization phenomenon inside a Vosgues sandstone in a triaxial cell. Int. J. Rock Mech. Min. Sci. 2000;37:1123–237.
[42] Bandis SC, Lumsden AC, Barton N. Fundamentals of rock joint deformation. Int. J. Rock Mech. Sci. Geomech. Abstr. 1983;20:249–68.
[43] Pan XD, Hudson JA. A simplified three dimensional Hoek–-Brown yield criterion. In: Romana, editor. Rock mechanics & power plants. Rotterdam: Balkema; 1988. p. 95–104.
[44] Fang Z. A local degradation approach to the numerical analysis of brittle fracture in heterogeneous rocks. PhD thesis, University of London, UK, 2001.
[45] Fang Z, Harrison JP. Development of a local degradation approach to the modelling of brittle fracture in heterogeneous rocks. Int. J. Rock Mech. Min. Sci. 2002;39:443–57.
[46] Pinto da Cunha A, editor. Scale effects in rock engineering—an overview of the Loen Workshop and other recent papers concerning scale effects. Proceedings of the Second International Workshop on Scale Effects in Rock Masses, Lisbon. Rotterdam: Balkema; 1993. p. 3–14.
[47] Panet M. Le calcul des tunnels par la méthode des curves convergence-confinement. Paris: Presses de l'École Nationale des Ponts et Chaussées; 1995.
[48] Salençon J. Contraction quasi-statique d'une cavité à symétrie sphérique ou cylindrique dans un milieu elastoplastique. Ann. Ponts Chaussées 1969;4:213–36.
[49] Fairhurst Ch. General philosophy of support design for underground structures in hard rock. In: Sinha S, editor. Underground structures: design and construction. Developments in geotechnical engineering series, 59B. Amsterdam: Elsevier; 1991.
[50] Carranza-Torres C. Self similarity analysis of the elasto-plastic response of underground openings in rock and effects of practical variables. PhD thesis, University of Minnesota, 1998.
[51] Carranza-Torres C, Fairhurst Ch. The elasto-plastic response of underground excavations in rock masses that obey the Hoek–Brown failure criterion. Int. J. Rock Mech. Min. Sci. 1999;36(5):777–809.
[52] Carranza-Torres C. Elasto-plastic solution of tunnel problems using the generalized form of Hoek–Brown failure criterion. Int. J. Rock Mech. Min. Sci. 2004;41(3):480–1 (Proceedings of the ISRM SINOROCK 2004 Symposium).
[53] Dormand JR, Prince PJ. A family of embedded Runge–Kutta formulae. J. Comput. Appl. Math 1980;6:19–26.
[54] ROCSCIENCE. Roclab user's guide. Toronto, Canada: Roscience, Inc.; 2002.
[55] Kovari K. On the existence of NATM, Erroneous concepts behind NATM. Tunnel no. 1, 1994.
[56] Lunardi P. The design and construction of tunnels using the approach based on the analysis of controlled deformation in rocks and soil. Tunnels Tunnelling Int. 2000:3–30.
[57] Lombardi G, Amberg WA. Une méthode de calcul elasto-plastique de l'état de tensión et de déformation autour d'une cavité souterraine. Third ISRM Congress, Denver, 1974. p. 1055–1060.